Lessons learned in autoclave synthesis of upconversion nanoparticles: unreported variables and safety considerations

Rebecca McGonigle,[†] Jodie Glasgow,[†§] Catriona Houston,[†] Iain Cameron,[†] Christian Homann,[††] Dominic J. Black,[‡] Robert Pal,[‡] Lewis E. MacKenzie[†]*

[†]Department of Pure and Applied Chemistry, University of Strathclyde, Glasgow, G1 1RD, United Kingdom.
[††] Department of Chemistry and Biomolecular Sciences, University of Ottawa, Ottawa, Ontario, K1N 6N5, Canada.
[‡] Department of Chemistry, Durham University, Durham, DH1 3LE, United Kingdom.
[§] Now at the Department of Chemistry, University of Manchester, Manchester, M13 9PL, United Kingdom.

*Corresponding author. Email: l.mackenzie@strath.ac.uk

Abstract

Autoclaves – vessels for sustaining high temperatures and high pressures – are widely used across chemical and biological sciences, and are one of the more accessible pieces of equipment for synthesis of luminescent upconversion nanoparticles (UCNPs) amongst other nanomaterials. Yet, despite being crucial to nanomaterial synthesis, the details of autoclave reactors used are barely reported in the literature, leaving several key synthesis variables widely unreported, and thereby hampering the reproducibility of many synthesises. In this perspective, we discuss the safety considerations of autoclave reactors and note that autoclaves should only be used if they are (a) purchased from reputable suppliers/manufacturers and (b) have been certified compliant with relevant safety standards. Ultimately, using unsuitable autoclave equipment can pose a severe physical hazard and may breach legal workplace safety requirements. In addition, we highlight a number of parameters in autoclave synthesis that we suggest should be reported as standard in order to maximise the reproducibility of autoclave synthesis experiments. Subsequently, we discuss two case studies where a commercially available high-safety autoclave system was used to synthesise UCNPs. We also provide broader context for the physical and optical properties of UCNPs, their applications, and other UCNP synthesis methods. We hope that this perspective encourages users of autoclave synthesis, whether in nanomaterials or in broader contexts to: (a) adopt and report the use of high-safety autoclaves and (b) report the many experimental variables involved in autoclave use to enhance reproducibility and robustness of nanomaterial synthesis.

1. Introduction

1.1. UCNP properties

Upconversion nanoparticles (UCNPs) are inorganic crystalline nanostructures consisting of a low-photon energy host lattice doped with photonically-active trivalent lanthanide ions. The host lattice is often $NaYF_4$ (either cubic (α) and hexagonal (β) phase). However a plethora of alternative host lattice materials have been explored.[1,2] The long-lived excited states of the lanthanide ions (typically ~100 µs to ~10 ms)[3] enables multi-photon absorption and subsequent upconversion process, where multiple low-energy photons are absorbed and converted into a higher energy photon.[4]

The constituent ions within UCNPs play a vital role in their photonic properties and eventual applications. Yb^{3+} and Nd^{3+} are common sensitizers in UCNPs, absorbing photons at near-infrared (NIR) wavelengths of 976 nm and 808 nm respectively, whereas UCNPs heavily doped with Er^{3+} can be excited at 808 nm, 975 nm, and 1532 nm.[5,6] Er^{3+} and Tm^{3+} are common emissive activator ions, with Ho^{3+}, Sm^{3+}, and Pr^{3+} being less commonly explored. In terms of emission, a comprehensive exploration of dopant combination influence on emission wavebands/colour has been provided by Chan et al., (2012).[7] Emission is generally achievable in "line like" discrete wavebands, from ultraviolet to NIR wavelengths.[8,9] Further, co-doping UCNPs with transition metals such as Mn^{2+} and Fe^{3+} can serve to enhance the efficiency of the upconversion process by (a) altering unit-cell size and (b) influencing multi-photon excitation and emission pathways.[10–13] Beyond purely optical properties, dopants also enable multi-modal responses, for example incorporation of Gd^{3+} and Dy^{3+} within or onto UCNPs induces a parametric response for magnetic resonance imaging (MRI) contrast[14] complimentary to x-ray computed tomography (CT)[15]; and incorporation of isotopes such as Fluorine-18 within UCNPs enables positron electron tomography (PET) response (see Figure 1).[16]

Core/shell architectures can be highly advantageous for UCNPs (see Figure 1). For example, it is well known that solvents containing OH^- groups, such as water or alcohols, can reduce UCNP emission by interfering by the non-radiative inter-ion energy transfer upconversion processes.[17] To counteract such detrimental effects, passive shell layers (e.g. of silica, $NaYF_4$, $NaLnF_4$, CaF_2, etc.) can be used to shield photonically active UCNP constituents. Shell layers can also be used to separate out functional dopants that would otherwise interfere with each other (e.g. Dy^{3+}can cause energy loss from Yb/Er systems if not properly isolated).[15] Carefully designed and synthesised photonically active shell architecture can enable advanced multi-wavelength excitation, e.g. for display technologies.[6,18]

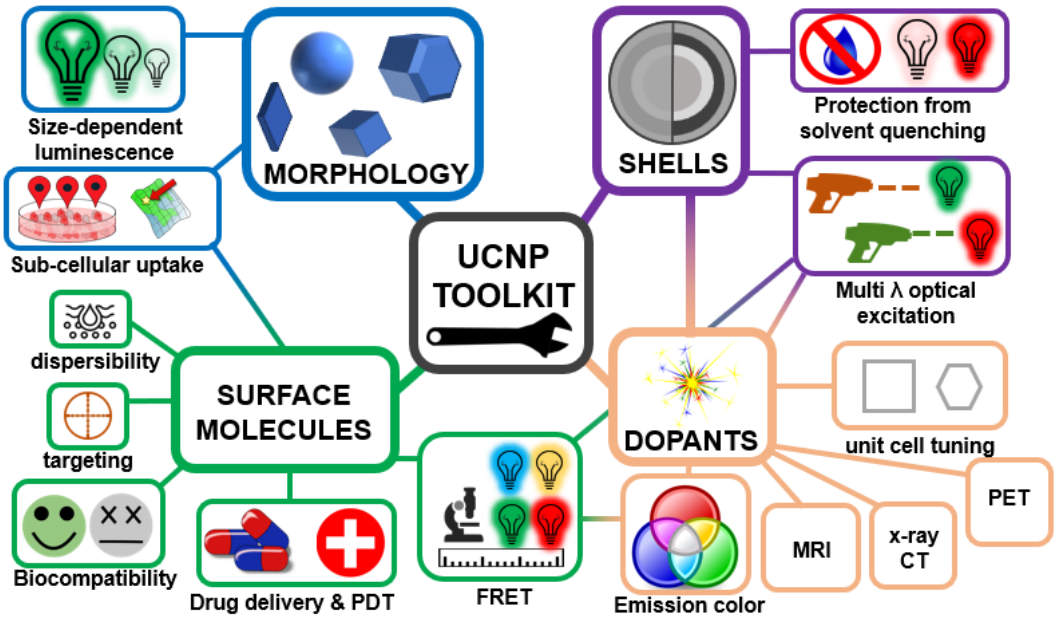

Figure 1. An overview of some of the many properties of UCNPs that can be achieved by altering UCNP synthesis parameters.

UCNPs offer several key advantages over other optically active materials, such as fluorescent dyes and quantum dots. Prominently, UCNPs do not photodegrade, photobleach, or blink.[19–23] This makes UCNPs well suited to application nanoscale temperature sensing,[24] pressure sensing,[25,26] transparent multicolour volumetric display technologies,[6,27] and lanthanide-based nanopatterned security inks.[28–30] In biological environments, the diffuse NIR UCNP excitation can travel through several millimetres of blood,[5] and several centimetres of *ex vivo* tissue due to minimal absorption and scattering at NIR wave ranges.[31–33] Further, NIR excitation does not induce visible autofluorescence, and has low phototoxicity.[34] The combination of these optical properties make UCNPs uniquely suited to all-optical reporting in life sciences applications.

Despites these substantive advantages, UCNPs suffer from poor light absorption of sensitizer ions such as Yb^{3+} and Nd^{3+}, and overall low photoluminescence quantum yield. The highest reported upconversion quantum yield for UCNPs was 10.3% for core/shell hexagonal-phase $NaYF_4$:18 %Yb^{3+},2 %Er^{3+} UCNPs in a dry form reported by Homann et al., (2018).[35] Indeed, hexagonal-phase UCNPs are generally favoured due to their higher efficiency of photon production over alpha phase UCNPs. More typical quantum yields for UCNPs in non-polar solvents are ~0.01% to 0.1%.[36] However, in our experience, the quantum yield of UCNPs dispersed in water may be orders of magnitude less. Whilst highest quantum yields are typically achieved with hexagonal-phase host lattice structures, it is worth noting that for the cubic phase $NaGdF_4$ the smallest UCNPs (below 20 nm in diameter) reportedly have an enhanced quantum yield compared to the hexagonal phase due to unexpected crystal lattice distortions.[36] For comparison, the quantum yield of rhodamine 6G is 95% in EtOH and the quantum yield of quantum dots is variable depending on the material, but 25-75% is typical with quantum yields as high as 95% being achieved for some quantum dot materials.[37,38] Unlike down-conversion systems (i.e. conventional fluorophores), it should be noted that two-photon And three photon upconversion processes will never exceed 50% and 33% quantum yield respectively. Nevertheless, there are reports of bright luminescence from well-optimised UCNPs being visible to the naked eye.[39,40]

UCNP absorption cross-section can be enhanced by incorporating NIR fluorescent dyes that enhance photon absorption and excite the UCNPs, thereby boosting overall UCNP emission, potentially by orders of magnitude.[41] The dye-UCNP interactions are mediated on the basis of Förster/Fluorescence Resonance Energy Transfer (FRET), with the details being best covered by other publications.[42,43] Notably, combining multiple fluorescent dyes can enable wavelength-selective UCNP excitation across the entire visible spectrum.[44] However, it should be clearly noted that NIR fluorescent dyes can photobleach on the timescale of minutes to tens of minutes under laser irradiation due to degradation by self-generated triplet-induced singlet oxygen,[45,46] so whilst potentially advantageous, the use of NIR fluorescent dyes over purely-inorganic core/shell UCNPs must be carefully considered. Further, some of the fluorescent dyes reported are not "off the shelf" and rather synthesised and modified in a bespoke and highly involved manner. Further, multiple different dyes may have synonymous names, e.g. various different dyes are known as 'IR-806' in the literature and may differ from commercially available dyes of the same name. Therefore close attention needs to be paid to the source and modifications of any dyes used in UCNP sensitization studies.[47–51] The advancements and prospects of fluorescent dye loaded UCNPs is best covered in a recent comprehensive review by Liu et al., (2023).[52]

Another approach to enhancing UCNP luminescence is to exploit plasmonic enhancement effects by bringing UCNPs into proximity to metallic nanoparticles or metallic surfaces of various morphologies. These materials are typically silver or gold and the approaches rely on the plasmon resonance of such materials being in resonance with the absorption of UCNP sensitizers, e.g. 976 nm for Yb^{3+} doped UCNPs. These approaches are well set out in a recent review by Liu et al., (2023).[53] Even more recently, Zhang et al., (2024)[54] used optical trapping to examine the effects of Brownian motion on plasmonic enhancement of UCNP in water.[54] Beyond emission enhancement for its own sake, plasmonic approaches can be exploited for biosensing at the interface of chirality .[29,55–57]

Surface ligands have a significant influence on the dispersion of UCNPs in solvents and how the nanoparticles are further functionalised. For example, oleic acid (OA) is commonly used in UCNP synthesis and enables dispersal in non-polar solvents. A number of other surface ligands enable dispersion in water, including citrate,[58,59] polyethylene glycol (PEG),[60] polyacrylic acid (PAA)[61], polyethyleneimine (PEI), and polyvinylpyrrolidone (PVP) (although PVP also enables dispersal in a wide range of organic solvents). [62,63] Whilst some ligands are intrinsic to the UCNP synthesis method, ultimately ligands may be replaced, substituted, or otherwise combined as needed to achieve a desired funcitonality.[58,64] Polymers such as PEI may be particularly attractive because they can provide multiple functionalities, such as protection of UCNP emission by excluding solvents, whilst offering routes for functionalisation of polymer moieties. Additionally, polymers can aid cellular uptake, and can offer routes to persistent cell and tissue labelling.[62,64–67] Drugs and other molecules can be loaded onto UCNPs to track drug delivery or achieve photodynamic therapy approaches.[68,69] Combing UCNPs with bio-recognition molecules such as antibodies and aptamers can enable specific binding of dyes, quantum dots, proteins, or other analytes for biosensing.[43,70–75] UCNPs systems can even be "camouflaged" with endogenous cellular membranes to enable immune system evasion *in vivo*.[76]

1.2. Historical trends in UCNP research

The body of literature on UCNPs is dizzying in scope (see Figure 2). From the 1960s, upconversion research mainly focused on bulk upconversion materials, with $NaYF_4$:Yb,Er emerging as the upconversion material of choice.[4] In the mid-2000s, UCNPs started appearing in the literature, somewhat lagging behind publications featuring *"nanoparticles"* more generally. Up to 2017, the number of publications featuring "*upconversion nanoparticles*" increased exponentially year-on-year, mirroring the wider report of publications featuring "*nanoparticles"*. This pattern is mirrored for related search terms such as *"UCNPs"* and *"upconversion nanocrystals".* Subsequently, the number of

publications on UCNPs appears to be declining year-on-year by a modest amount. This is in contrast to the wider field of "*nanoparticles*", which appears to be reaching a plateau.

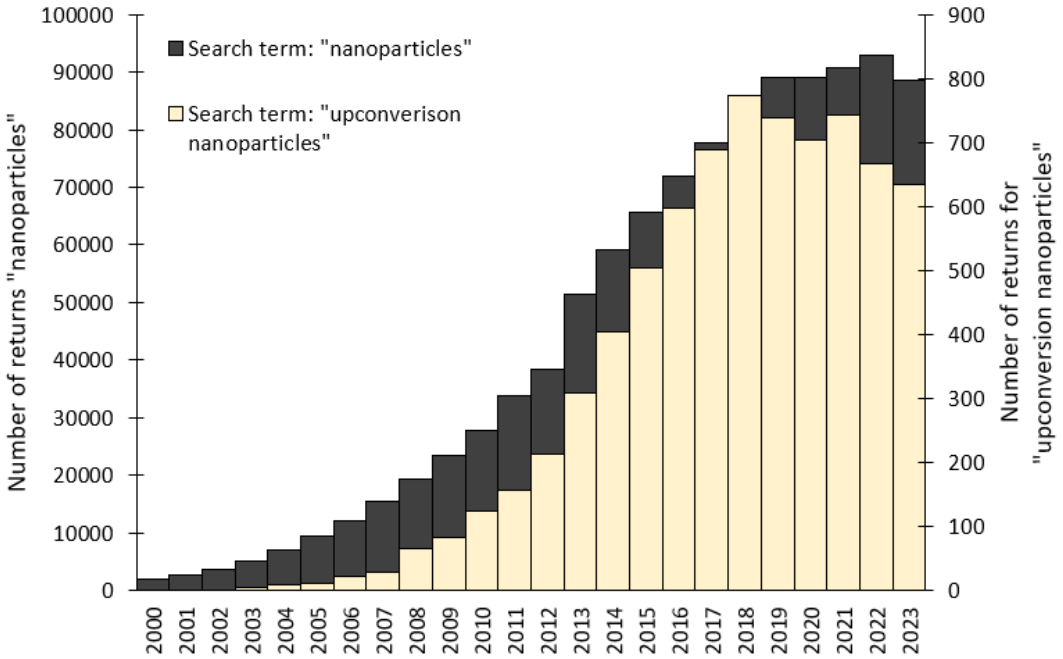

Figure 2. The annual number of publications indexed by *Web of Science*™ featuring the term *"upconversion nanoparticles"* (yellow bars) vs the number of publications featuring the search term *"nanoparticles*" (black bar). Data Copyright Clarivate 2024, all rights reserved. Figure is original.

1.3. Commercially sourcing UCNPs: problematic and prohibitively expensive

Despite their utility, UCNPs are extremely expensive to purchase, arguably prohibitively so. For example, in mid-2023, a leading chemical supplies company listed 10 mg of OA coated $NaYF_4$:Yb,Er UCNPs at a cost ~£320 + 20% VAT. From the same major supplier, core/shell $NaYF_4$,Yb,Tm@$NaYF_4$,Yb,Nd UCNPs with dual-wavelength excitation (808 nm and 976 nm) were listed at £780 + VAT for 10 mg. Further, core/dual-shell UCNPs with a $NaYF_4$:Tm core, a passive $NaYF_4$ shell, and a silica outer shell will cost £5940 + VAT for 10 mg. These costs will likely make purchasing the required quantities of UCNPs for various applications prohibitively expensive. Further, despite the price of UCNPs, it seems that major chemical supply companies offer little in the way of quality assurance or continuous availability of UCNPs. For example, the aforementioned leading chemical supplies company only stated UCNP surface ligands, approximate diameter, and peak of emission waveband(s). There is no information about UCNP size distribution, no representative UCNP spectrum, and no electron microscopy images demonstrating UCNP morphology: all very important parameters for UCNP applications. Further, during the process of writing this manuscript, the majority of the UCNPs products discussed herein were withdrawn from the market without notice to consumers. This highlights the unpredictability of sourcing UCNPs commercially.

When considering purchasing UCNPs it is also necessary to consider what quantity is needed. For example, quantum yield estimation typically requires 75 mg of UCNPs.[36] Whereas for *in vivo* studies, doses of 100 mg/kg of bodyweight may be administered to a mouse. Given that a typical mouse may weigh ~20 g, this requires only 2.5 mg of UCNPs. However, such studies may require repeated UCNP dosage for many days with many animals, the quantity of UCNPs required will quickly add up. A good example is an *in vivo* biocompatibility/UCNP tolerance study reported by Zhou et al., (2019)[77] in which

$NaYF_4$:Yb/Er@SiO_2 UCNPs were administered to 36 mice (average weight 22 g) for up to 14 consecutive days at UCNP doses of 20 mg/kg and 100 mg/kg of bodyweight. We estimate that this study would have required ~360 mg of $NaYF_4$:Yb/Er@SiO_2 UCNPs, assuming zero wastage. Assuming $NaYF_4$:Yb/Er@SiO_2 UCNPs could be procured at a cost of £700 for 10 mg (excluding V.A.T.) we estimate that 360 mg of such UCNPs would cost in excess of £25,000. This is an extremely large cost for research consumables.

Ultimately, these factors combine to make commercial procurement of UCNPs extremely risky and expensive for a research project. Consequently, reliable and repeatable on-demand synthesis of UCNPs is not only desirable, but absolutely necessary for reproducible UCNP studies across the sciences.

2. UCNP synthesis methods

2.1.1. Motivation, scope, and context

UCNPs synthesis is not trivial. At minimum, UCNP synthesis requires a chemical laboratory to facilitate safe handling of various chemicals and ensure adequate ventilation. Some techniques require minimal skill and are consistently reliable (e.g. PVP assisted synthesis).[2,10] Yet several of the most widely used UCNP techniques require a nuanced understanding of the synthesis, and a considerable deal of operator skill to control the variables involved. To help frame our discussion, we have created a "skill ladder" of UCNP synthesis, up which a research group or experimental operator may climb as they gain experience, skills, and resources (see Figure 3).

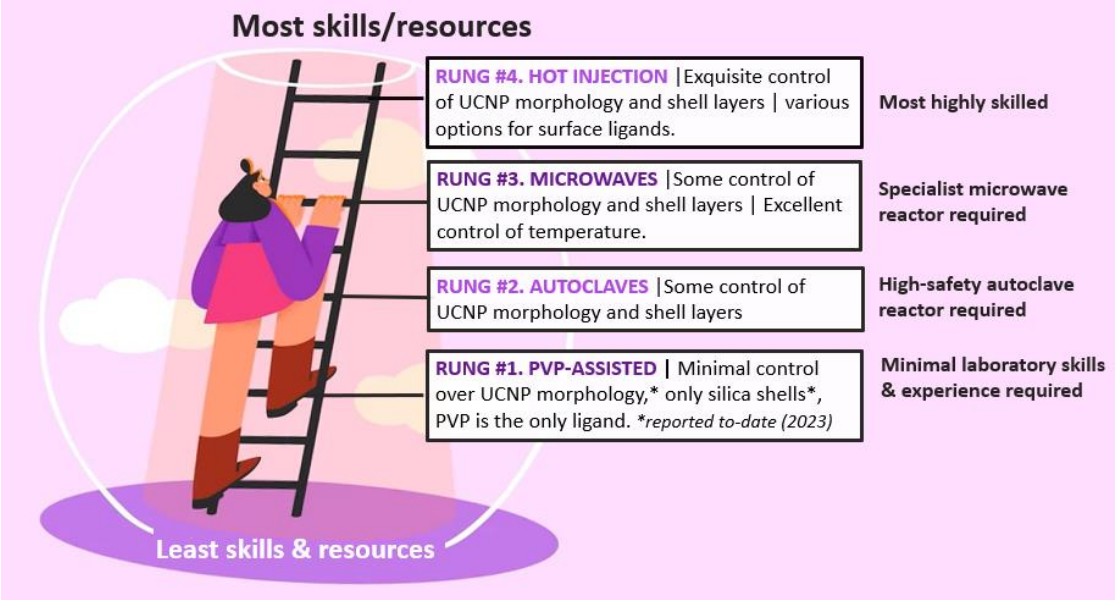

Figure 3. A diagram representing the "skill ladder" associated with UCNP synthesis. The higher up the ladder one climbs, the more skills, resources, and experience are required.

At this point, we note that our perspective and discussion focuses on synthesis methods which produce UCNPs that exhibit luminescence in colloidal suspensions. Therefore, we have excluded from discussion: (a) synthesis of bulk materials; (b) synthesis of micro-materials; (c) any processes involving high-temperature dry annealing to improve crystallinity of UCNPs; and (d) studies where upconversion luminescence is only reported in dry form.[78] For reasons of scope, we have also excluded some lesser-used UCNP synthesis techniques, such as ball milling and continuous reactors. For these approaches, readers are referred to a review by Jiao et al., (2020).[79]

2.1.2. Low-temperature UCNP synthesis techniques

There are some intriguing room-temperature UCNP synthesis techniques which are currently under-explored and do not strictly fit the scope for the wider context of this perspective. Nevertheless, they may offer value for future exploration, so we highlight them here. For example, ultrafast (~1 minute) room-temperature synthesis of bare $NaBiF_4$:Ln upconversion nanomaterials has been reported by Lei et al (2017)[80] and Du et al., (2018).[81] In our own – unpublished – attempts to reproduce these methods, we found that upconversion in EtOH was detectable, but extremely weak, likely due to solvent quenching. One could envision scenarios where upconversion of such UCNPs could be enhanced by (a) simple dispersal in non-polar solvents, or (b) by forming a protective inert shell or polymer layer around the $NaBiF_4$:Ln UCNPs. Nevertheless, room temperature synthesis of UCNPs is exceptional because UCNP synthesis typically requires temperatures between 180 and 310 °C.[79]

Also at an unusually low-temperature, Shao et al., (2014)[78] reported a layer-by-layer nanosheet process for forming beta-phase (hexagonal) $NaYF_4$:Ln UCNP nanorods with a 3 hour reaction step at the exceptionally low temperature of 50°C.[78] These $NaBiF_4$:Ln UCNPs reportedly showed upconversion emission in EtOH. Intriguingly, Liang et al., (2007)[82] reported formation of α-phase NaYF4 nanocrystals at room temperature, with a very indistinct X-ray diffraction pattern forming indicating poor crystallinity; upconversion emission via this room-temperature host lattice formation was not investigated.[82] More recently, Lei and Zhang (2021)[83] produced hollow $NaBiF_4$:Yb,Er UCNPs in a one-pot room-temperature synthesis via a "liquid nanoparticle" approach, although it is unclear if these UCNPs are suitable for dispersal in solvents.[83] Further investigation of these synthesis methods could be beneficial for "green" UCNP synthesis or synthesis of UCNP at larger scale.

2.2. PVP-assisted UCNP synthesis

Perhaps the simplest route of producing UCNPs is the polyvinylpyrrolidone (PVP) assisted route, requiring only basic laboratory equipment. The PVP UCNP synthesis route was first reported by Li and Zhang in 2006,[63] who proposed a UCNP formation mechanism where Ln^{3+} ions coordinate with the hydrophilic pyrrolidone moiety of PVP, thus forming nucleation sites for UCNP growth. The primary reaction in this procedure can be conducted open-to-air in round bottom flasks (160 °C for 2 hours) with simple hot-plate stirring/heating apparatus that is readily accessible in many wet laboratories. We have found it typically produces ~130 mg of PVP-coated UCNPs with a typical diameter of ~50 nm.[2,10,63] These PVP UCNPs can be dispersed in a wide range of solvents, e.g. water, ethanol, methanol, isopropanol, chloroform, DMSO, DMF, etc; and can also be functionalised with silica shells.[63] A wide range of emission colours have been demonstrated, including red, green, and blue emission achieved via co-doping with various combinations of Yb^{3+}, Er^{3+}, Tm^{3+}, and Mn^{2+}.[2,10,63] Typically PVP-UCNPs appear pseudo-spherical or pseudo-cuboidal, but their morphology can be altered by Mn^{2+} co-doping, producing smaller and less homogenous UCNPs that may indicate a non-uniform UCNP formation process, similar to hollow UCNPs reported by others.[83] Scale-up of PVP-UCNP synthesis could likely be achieved via parallel batch synthesis or a with a larger reaction vessel; attractive for large-scale applications such as light-harvesting in solar cells, display technologies, commercial biosensors, and security inks.[10,67]

Jin et al., (2011)[64] noted that PVP-coated UCNPs had good biocompatibility.[64] However, the PVP-UCNP synthesis does have some inefficiencies that should be noted. Firstly, it involves a seemingly redundant heating and drying step to convert lanthanide oxides (Ln_3O_2) in 10% HNO_3 to lanthanide nitrates ($Ln(NO3)_3$). This is inefficient because the lanthanide oxides are poorly soluble in 10% HNO_3 and so it may take some time (on the order of days) for full dissolution of concentrated stock solutions. It is apparent that starting with readily soluble lanthanide nitrates would be more efficient. However in our experience this does not result in the formation of PVP-UCNPs for unclear reasons. Secondly,

the degradation of nitrates under heating produces orange-coloured fumes, which is presumed to be NO_2.[10,84] Thirdly, whilst convenient, the that open-to-air synthesis may result in oxygen vacancies in the $NaYF_4$ host lattice (i.e. oxygen competing with fluorine) thereby altering/reducing upconversion efficiency.[85] Finally, the origin of rhombus-shaped PVP-UCNPs observed by Birch et al., (2023)[2] is unclear. Electron microscopy diffraction and non-quantitative elemental mapping analysis indicated that these rhombus-shaped nanoparticles are composed of cubic-phase $NaYF_4$:Yb,Er. However, rhombus shaped nanoparticles are more commonly associated with YF_3 structures that are formed in reactions where Na^+ is scarce. Further research into the formation of the rhombus-shaped PVP-UCNPs is warranted, and may benefit from single-nanoparticle analytical techniques.[2,86] In the broader context, the quantum yield of PVP-UCNPs has not yet been measured and benchmarked against other upconversion materials; action is needed to address this important point of comparison.

2.3. Autoclave synthesis of UCNPs

Autoclaves – vessels for sustaining high temperatures and high pressures – are widely used across chemical and biological sciences, and are arguably one of the more accessible apparatus used for synthesis of UCNPs. Autoclaves are used in many aspects of chemistry and materials science, including synthesis of many types of nano and micromaterials,[87,88] metal organic frameworks,[87] catalysis,[89] hydrogenation,[90] polymerisation,[91] materials testing,[92] digestion,[93] single-crystal casting,[94] and corrosion testing.[95] In our opinion, autoclave UCNP synthesis is an affordable route to producing UCNPS with many relevant synthesis procedures reported in the literature. However, UCNP synthesis with autoclaves requires (a) detailed consideration of safety (see Section 2.3.1) and an understanding of often unreported autoclave synthesis variables (see Section 2.3.2).

2.3.1. Autoclave design, safety, and legality considerations

In the context of nanoparticle synthesis, autoclave reactors can be reductively described as extremely strong enclosed metal vessels, designed to contain reaction mixtures at elevated temperatures and pressures. Autoclaves serve as the “pot” in which many hydrothermal and solvothermal reactions occur.

Safety is a major concern with pressurised autoclave reactors, because an autoclave failure or erroneous opening under pressure can result in the release of large amounts of energy and/or heated fluids (i.e. an explosion). The hazards associated with autoclave synthesis are compounded (a) the design of the autoclave and (b) the type of reaction occurring inside the autoclave and resultant pressure build-up. In hydrothermal UCNP synthesis reactions approaching 100°C, water will of course form steam, which generates an elevated pressure (we typically record 10 to 25 bars of pressure in such hydrothermal syntheses). In solvothermal reactions, UCNP synthesis will only generate excess pressure if heated to temperatures excess of the boiling point of the solvents used, e.g. ethylene glycol [197°C], oleic acid [286°C], and 1-octadecene (ODE) [178-179°C] at standard atmospheric pressure.[96–98] Therefore at typical autoclave synthesis temperatures (180-200°C), solvothermal synthesis (assuming dry starting products) will not generate excess pressure.

Autoclave designs generally range from relatively simple screw-thread systems, to more sophisticated safety systems incorporating multiple redundant safety features (see Figure 4a and 4b respectively). Generally, all autoclaves include a liner (e.g. PTFE or suitable glass) where the reaction mixture is situated. The simplest autoclaves can be heated in an oven or heated in parallel with a heating block and feature an over-pressure disk. With such systems, care must be taken to preserve integrity of screw threads and to ensure there is not excess pressure contained within the reactor before it is opened. However, if the autoclave does not have pressure gauge or internal temperature reading system, then one must have to rely on good judgement of the operator. Therefore, such simple autoclaves have higher risks of accidental failure.

More advanced high-safety autoclave reactor systems will feature engineering controls to help ensure safety. As a minimal example, the Berghoff DAB pressure vessels (see Figure 4a) include a rupture disk to release pressure beyond tolerances.[99] Manufacturers also offer more sophisticated high-safety autoclave reactor systems. For example, both the Berghoff DB series and Asynt PressureSyn series (see Figure 4b) offer high safety reactors that use clamps instead of threads, pressure release valves, and over-pressure bursting disks, temperature probe ports, and pressure gauges.[100,101] These features allow operators to identify and control potential pressure hazards during operation. Therefore, there is lower risk of misuse.

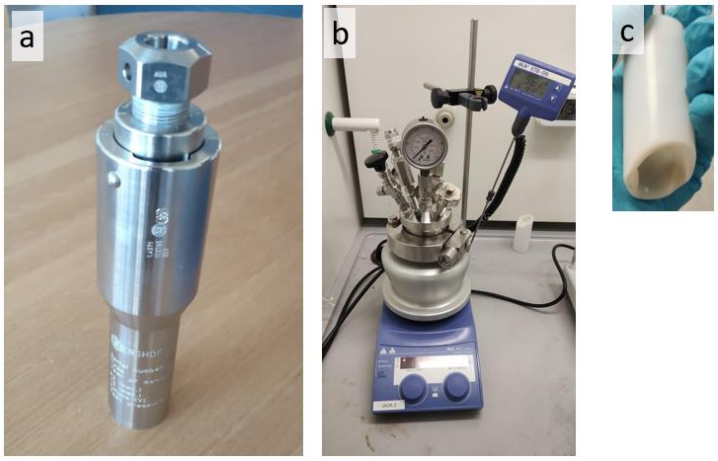

Figure 4. Examples of autoclave reactor systems. (a) a screw-thread Berghoff Digestec DAB autoclave reactor (photo courtesy of Dr Juliane Simmchen). (b) an assembled Asynt PressureSyn high-safety autoclave reactor and hotplate heating block situated on a hotplate stirrer within a fume hood. (c) a PTFE liner which was deformed due to the following process: (1) some liquid was erroneously left between the liner and metal autoclave, (2) this caused inefficient heating of the reaction mixture, resulting in the heating control system to apply a consistently elevated heating temperature, (3) resulting in excessive heating of the liquid, (4) elevating temperatures to a point where the PTFE softened and deformed.

Autoclave reactors can be heated by a number of means, including heating blocks and ovens. Manufacturers are now offering multiple autoclave heating options with specialised heating blocks and associated handling systems. Such systems are space efficient and include temperature control via probes inside the reaction vessel itself alongside magnetic stirring. Notably, the most advanced systems available remove the need for manual-handling, thereby preventing burn hazards and allowing maximum accessibility to all users – after all, autoclaves are made from solid metal (e.g. stainless steel) and are therefore cumbersome and difficult for many to handle. The most advanced autoclave reactor systems also enable automated temperature data logging and feature active cooling in order to recover products faster than passive cooling will allow, thereby increasing potential synthesis rate, and enabling safety features such as automatic shut-down if nearing maximum limits. Not only is this data-driven approach convenient and safe, but it also helps to enable reproducible synthesis.

Autoclaves reactors can facilitate synthesis at various scales, with systems ranging from 10 mL to 500 L on the market. Some manufacturers offer metal-free autoclave reactor chambers (i.e. where the reaction sleeve is totally contained), and some manufacturers offer autoclaves with multiple reactors, allow parallel batch synthesis of different UCNP compositions. Multi-chamber reactors are desirable for optimising UCNP synthesis in a shorter time-period.

To summarise: contemporary high-safety autoclave systems offer benefits in terms of (a) safety, (b) accessibility, and (c) reaction monitoring. Further, more sophisticated autoclave systems with larger or multiple reaction chambers may also help reduce time required to iterate synthesis towards optimisation or simply enable the generation of greater quantity of desired product.

Some additional "last line of defence" measures above standard laboratory procedures may be considered for best safety practice when using autoclaves. (1) a form of secondary shielding around the autoclave system to protect operators; some autoclave reactor manufacturers sell appropriate products, e.g. polycarbonate safety shields. (2) Provision of hearing protection for operators in case of rupture of an over-pressure burst valve (if one is used).

The maximum heat and pressure a given autoclave can safely sustain is primarily determined by the materials it is manufactured from (often stainless steel, with other options on the market including alloys, glass, nickel, titanium, and zirconium options). However, it is worth noting that PTFE liners are known to soften and deform if exposed to sufficiently high temperatures and pressurises arising from erroneous usage (see Figure 4c). Instead, liners made of borosilicate glass or other alternative materials may be required to reach maximum performance temperature. Autoclave reactor manufacturers can often provide additional information about maximum reaction temperatures for a given liner material.

There are various regulations worldwide regarding use of pressurised equipment. In the UK, employers have a legal duty to comply with the 'Pressure Systems Safety Regulations 2000 (PSSR)' as part of the broader legal duties specified the 'Health and Safety at Work Act' (1974).[102–104] The PSSR regulation aims "*to prevent serious injury from the hazard of stored energy as a result of the failure of a pressure system or one of it's component parts*", and applies to any *"compressed or liquefied gas, including air, at a pressure than greater than 0.5 above atmospheric pressure*" and "*pressurised hot water above 110 °C"* .[102] There are some exceptions to the PSSR, which include (but are not limited to) pressure systems to be used for "weapons systems", "vehicle tyres", and "experimental research". However, we note that most research is conducted at universities who have a duty of care to their students and staff, so we suggest that it would be good practice to note ignore the PSSR when using autoclaves for nanomaterial synthesis research. In the European Union, the directive 2014/68/EU[105] governs the certification and testing of equipment pressurised to > 0.5 bar.[105] Guidance in other countries varies and cannot be comprehensively covered here. We encourage all users to autoclave reactors to (a) familiarise themselves with the legal requirements and guidance regarding autoclave reactors for their specific country, and (b) to source autoclaves which are compliant with the highest international standards.

Autoclave reactors should only ever be purchased from reputable scientific suppliers who pre-test and certify their autoclave reactors to governmental standards. Example of reputable manufacturers include (but may not be limited to): Berghof GmBH (Germany), Büchiglasuster (Switzerland), Asynt Ltd (United Kingdom), LBBC Baskerville Ltd (United Kingdom), Mettler Toledo (USA/global), and Parr Instrument Company (USA). It is also worth nothing that in our experience, some manufacturers will provide certification of testing but may not provide a user manual or equivalent example operating procedures. This can result in some unexpected issues for inexperienced users. For example, any

ferrules that are used to introduce thermocouple probes to autoclave reactor ports will likely become permanently conjoined with a thermocouple probe after autoclave usage. Further, appropriate high-temperature high-pressure grease (e.g. CRC Lithium Grease 30570 for temporary operation up to 200 °C) will aid smooth situation of clamp components, and non-flammable leak detector fluid (e.g. SNOOP®) can be beneficial to check that all fittings are secure and pressure is contained.

It should be noted that there are some dubiously low-cost autoclave reactors that are readily available via non-reputable manufacturers: these autoclave reactors will likely not be compliant with government standards at these low price points. Therefore, such low-cost represent a high degree of risk of spurious failure and therefore a high risk of lethal hazard and should not be used.

Ultimately, suitably certified autoclave reactors are a relatively affordable way of starting with UCNP synthesis, with many systems within the remits of typical small equipment grants. We strongly recommend that research teams purchase autoclaves from certified reputable suppliers, which meet governmental certification standards, and which include multiple redundant safety features.

2.3.2. The unreported variables in autoclave synthesis

A very large amount of studies report autoclave UCNP synthesis, yet most of these studies do not report how what autoclaves were used. For example, much of the literature simply states that reaction mixtures were "*added to a Teflon lined autoclave*" and *"heated at"* a temperature for some time. This raises many questions. What volume is the autoclave reactor? What is it made of? How is it heated? Was it pre-heated? Is the quoted temperature the internal reactor temperature or the external heater temperature? What timepoint counts as reaction onset? How much internal space does the liner occupy? Was the reaction stirred? What pressure did the reaction occur at? This is a huge parameter space of unreported variables. In our experience, this combinatorial pitfall of variables can make it difficult for researchers to reproduce a UCNP autoclave synthesis – particularly hydrothermal autoclave UCNP synthesis (see Section 2.3.3) – even when using the same autoclave equipment in the same laboratory environment. If it is challenging for researchers using the same equipment and reagents to reproduce, then how can we possibly reproduce UCNP synthesis studies where equipment used is fundamentally unreported? The absence of comprehensive reporting has the potential to waste significant time and effort within our research community. Therefore, in the interest of robust, reproducible, and open science we strongly recommend that a number of key autoclave parameters and variables are reported; these are summarised in Table 1.

Table 1. Key parameters and variable to report in autoclave synthesis of UCNPs in order to maximise reproducibility.

	Key parameter/variable	Importance
General autoclave operation	Make and model of autoclave reactor.	Reproducibility and repeatability by others.
	Make and model of autoclave heating system.	
	Maximum heat and pressure specified by manufacturers.	Understanding limits of reactor equipment.
	Reactor and sleeve cleaning procedure.	May help identify potential issues with contamination.
	Safety precautions.	Ensuring safety and sharing good practice.
Reaction containment and liner	Empty autoclave chamber volume.	Pressure of reaction depends on volume available for gas generation and expansion.
	Autoclave chamber volume once liner is inserted.	
	Volume of liner.	
	Total volume of reaction mixture added within liner (i.e. fill factor).	
	Liner material.	Influences heat transfer rate.
	Does the liner have a lid?	If not fully enclosed, gas may expand into autoclave headspace; possible contamination risk.
	Was an inert atmosphere introduced?	Inert atmospheres may benefit UCNP luminescence.
Stirring	Was the reaction mixture stirred? If so, at what rate?	May alter size of any micelles present in hydrothermal reactions.
	What size and shape of stir bar was used?	Influences chamber volume.
Heating and temperature	Autoclave construction and materials	Influences heat transfer rate.
	Heat source (e.g. oven, hotplate, heating mantle, etc)	Governs heating uniformity and heating rate.
	Heating control method and target temperature	Heat delivery rate is a key variable in synthesis.
	Is the heating control and target temperature based on internal or external temperature?	External temperature and reactor internal temperature are different due to heat differentials. Reactor internal temperature lags behind external temperature.
	Was the reactor pre-heated?	Influences heating rate and total energy in the system.
	When is the reaction timer deemed to have started?	Determines total energy input into the reaction mixture.
	Was temperature data logged as reaction occurred?	Aids repeatability and troubleshooting.
Pressure	Does the autoclave have a pressure gauge?	Pressure generated may be important for synthesis outcomes.
	What was the internal pressure during the reaction?	Pressure generated may be important for synthesis outcomes.

2.3.3. Case study #1: adapting a hybrid hydrothermal/solvothermal autoclave synthesis method to produce oleic-acid coated UCNPs (OA-UCNPs)

There is abundant literature on the hydrothermal synthesis of oleic-acid functionalised UCNPs (OA-UCNPs) using autoclaves. However, there are two major problems with reproducing hydrothermal OA-UCNP synthesis: (1) the underlying principles of the hydrothermal synthesis are usually not described, and (2) many autoclave synthesis variables – as outlined in Table 1 – have been historically unreported. In our experience, this has made it challenging and tedious to reproduce autoclave hydrothermal syntheses reported by other groups. Rather, published approaches have served as a starting point, with a great deal of refinement and optimisation research required to produce viable OA-UCNPs. In this case study we aim to convey an example of this process, the frustrations encountered, and the "lessons learned".

For the purposes of this case study, we adapted a procedure from Bi et al., (2022),[106] which reports the synthesis of cubic shaped $NaYF_4$:Yb,Er,Mn UCNPs with strong single-band red emission via hydrothermal autoclave reaction. The choice to adapt Bi et al., was somewhat arbitrary as we were simply aiming for monodisperse UCNPs ~50 nm in diameter with strong red emission. Importantly, in this scheme precursors are lanthanide chlorides ($LnCl_3$), and the Mn source is $Mn(CH_3COO)_2$. The reaction includes a small amount of aqueous 2M NaOH (1.5 mL), 10 mL "anhydrous alcohol", and 5 mL OA. It is believed that these reactants combine to form Na and RE oleates.[107] Rather than being purely hydrothermal, this is a biphasic system consisting of small reverse micelles of water within OA (and ODE if present)(see Figure 5).[107,108] Understanding the bi-phasic nature of "hydrothermal" UCNP synthesis was key to our understanding and control of the UCNP synthesis reaction, which we herein refer to as a "hybrid hydrothermal/solvothermal" reaction. At a suitably high temperature, the $Mn(CH_3COO)_2$ precursor thermally decomposes, resulting in UCNP nucleation events (N.B. precursor choice is an important topic in UCNP synthesis and is best covered in-depth by others).[109,110]

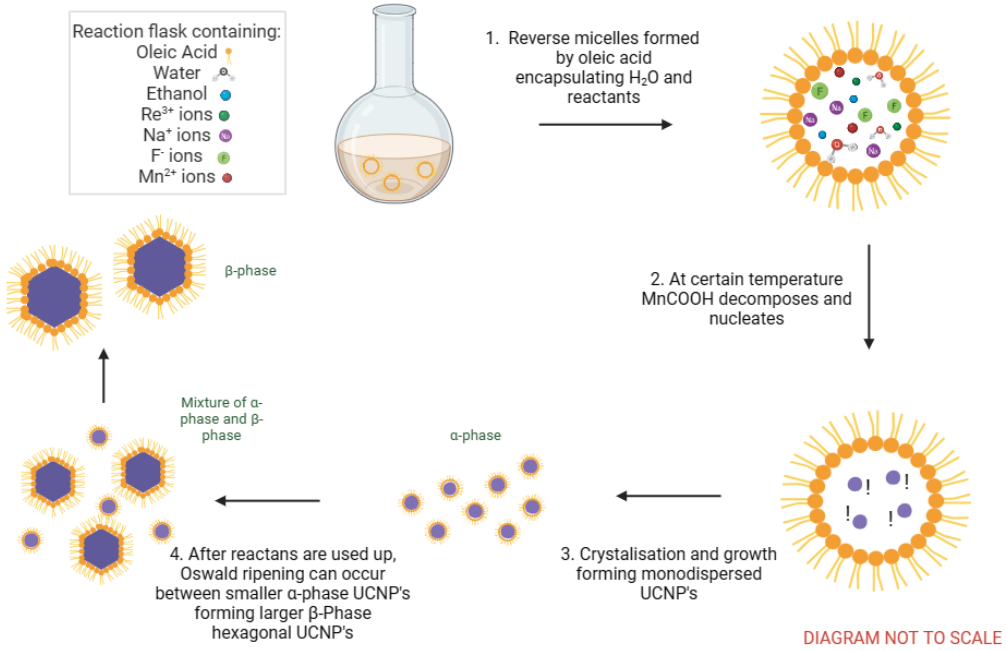

Figure 5. Hybrid solvothermal/hydrothermal reaction scheme for producing OA-UCNPs.

Like most studies in the field, Bi et al., gave a sparse description of their autoclave methods: i.e. "*a 50 mL stainless Teflon-lined autoclave*" which was "*continuously heated at 200°C for 8 hours*". We set about to reproduce results from Bi et al., for $NaYF_4$:Yb,Er,Mn (25 mol% Mn^{2+}) UCNPs using our Asynt PressureSyn high-safety autoclave reactor (see Figure 4b). In our initial procedure, we prepared stocks of NaOH, $RECl_3.6H_2O$, $Mn(CH_3CO_2)_2.4H_2O$, and NaF in deionised water and appropriate amounts were mixed with EtOH (Bi et al., specified "anhydrous alcohol"),[82] and OA; these were then stirred thoroughly before addition to the autoclave. Our use of stock solutions resulted in the addition of 10 mL more water than in Bi et al., where solid $RECl_3$ and $Mn(CH_3CO_2)_2$ starting materials were added directly to the reaction solution. Our Pressure Syn autoclave reactor system was a stainless steel autoclave reactor with a 125 mL total chamber volume and a lidless liner with a total maximum volume of ~80 mL volume. Heating was provided by an IKA RCT hotplate and a specialised heating mantle. The manufacturer states that this system provides uniform heating to the bottom and sides of the

autoclave reactor. An internal thermocouple attached to the autoclave was immersed within the reaction solution and was used to provide temperature control and feedback. All starting materials and solvent volumes were kept as close as possible to Bi et. al., and an atmospheric blanket of N_2 was introduced before sealing the autoclave reactor. Prior testing had indicated that reaction mixtures that are predominately OA would reach a maximum of 180°C in our autoclave reactor. Therefore, we initially set the target temperature to 190 °C to maximise heating rate (or to 200 °C if necessary), subsequently lowering the target temperature to 180 °C once the reaction mixture reached 180 °C. The reaction timer was started once the autoclave reactor internal temperature reached 120 °C (after ~30 minutes of heating) and the reaction subsequently proceeded for 8 hours before heating was disabled and the reactor was allowed to cool naturally. The reaction was not stirred. Pressure and temperature data was logged manually. The variation of reactor temperature, reactor pressure, heating mantle temperature, and hotplate output temperature are shown in Figure 6. After the reaction was complete, the products were recovered, washed, and analysed with electron microscopy and upconversion spectroscopy. The resulting UCNPs were curious: they exhibited strong red upconversion, but the nanoparticles were a mixture of nanorods and flat plates shapes (see Figure 7e). This was entirely unlike what was expected from Bi et al., (2022) and coincidentally more like LaF_3:Yb,Er nanoplates reported Liu et al., (2007).[111] Therefore, the reaction conditions required careful consideration and modification.

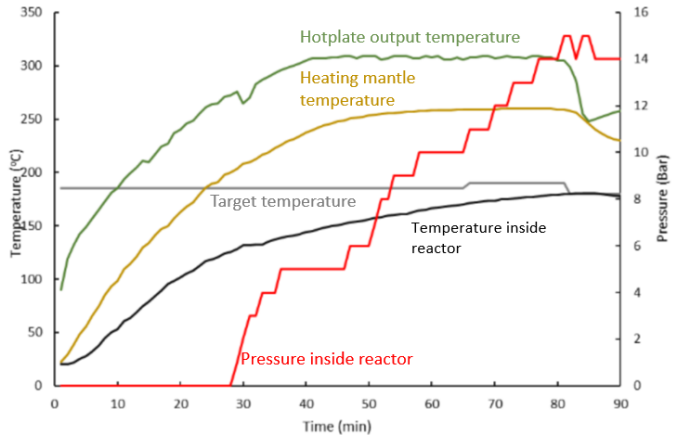

Figure 6. Heat and pressure of our Asynt PressureSyn autoclave reactor system during the initial phase of a typical hybrid hydrothermal/solvothermal UCNP synthesis.

Due to the bi-phasic nature of the hybrid hydrothermal/solvothermal reaction, we speculated the reaction could be improved by (a) removing as much water as possible from the synthesis and (b) purposefully and sequentially adding starting materials. First, 1.5 mL NaOH was mixed with OA for 1 hour by stirring at 700 RPM to form sodium oleates. Then stocks of $RECl_3.6H_2O$ pre-prepared in EtOH were added to the mixture. Finally, solid $Mn(CH_3CO_2)_2.4H_2O$ and NaF were added directly and slowly, before further stirring. We propose that this process mainly confines the majority of UCNP precursor material – including the important $Mn(CH_3CO_2)_2$ for thermal decomposition/nucleation – to within the reverse micelles. However, the reduced water content also reduced total reaction mixture volume which was problematic because the thermocouple probe (introduced via an angled port) could not be immersed into the reaction mixture! Therefore, the heat applied to the autoclave was controlled via the temperature of the heating mantle. From prior experience of monitoring both heating mantle and internal temperatures, we surmised that a heating mantle temperature of 200 °C would be

appropriate for reaching 180 °C inside the autoclave reactor. The reaction timer was started once the heating mantle reached 145 °C and the reaction was allowed to occur for a variety of time points.[a]

With this updated protocol, instead of the expected UCNP nano cubes, we produced UCNPs in a variety of shapes, dependent on reaction time. For a 2 hour reaction, small irregular "nanobean" shaped UCNPs were produced with a diameter of 26 ± 6 nm (maximum ferret diameter ± standard deviation) (see Figure 7a); 4 hours produced the aforementioned "nanobeans" with the addition of thin hexagonal plates forming (see Figure 7b); 8 hours produced rods with a hexagonal-face and ends that could be described as "crown like" were produced (266 ± 12 nm across the hexagonal face) (see Figure 7c,d). This UCNP formation processes has been reported in a number of other studies: the "nanobeans" are meta-stable α-phase (i.e. cubic) crystal lattice nanoparticles formed at relatively low temperatures, and which re-dissolve at higher sustained temperatures, resulting in the formation of more stable and larger β-phase UCNPs via Ostwald ripening (see references for detailed discussion).[108,110,112–114] When dispersed in cyclohexane, upconversion emission from the larger OA-UCNPs was much stronger than the smaller "nanobean" OA-UCNPs; this was attributed to reduction of size-dependent quenching via interaction with solvent molecules.[17,115]

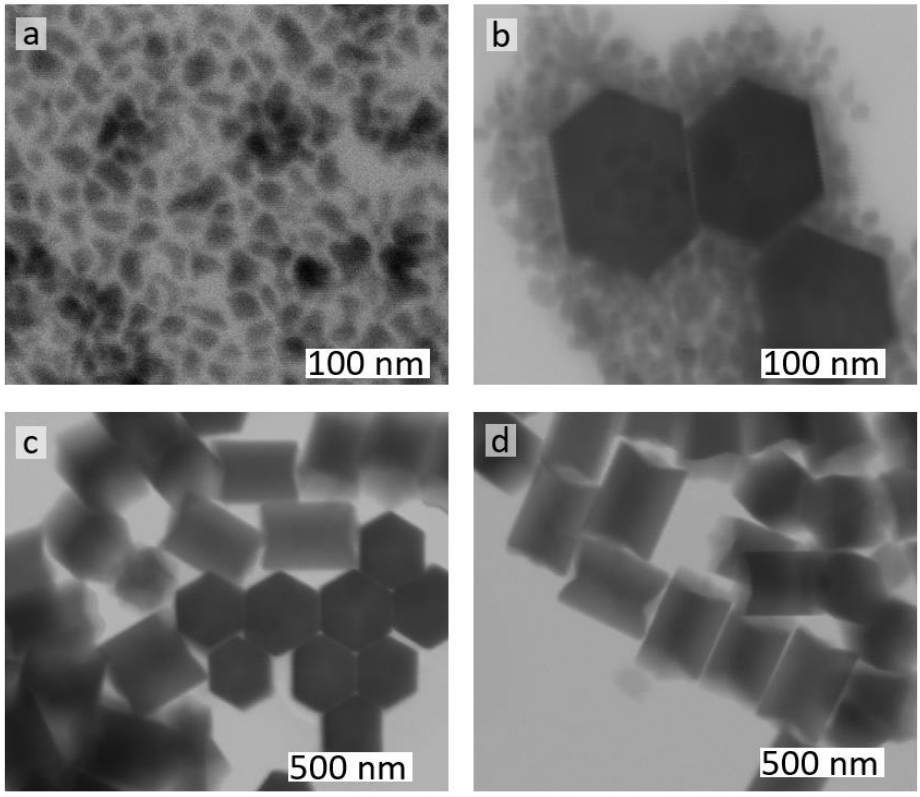

Figure 7. UCNPs produced by the hybrid hydrothermal/solvothermal synthesis described in Case Study #1. (a) 2 hour synthesis product: "nanobean" shaped. (b) 4 hour synthesis product. (c, d) 8 hour synthesis product.

Ultimately, despite successfully producing UCNPs, we spent a large number of person-hours optimising a synthesis procedure that have been well established in the literature since ~2007 onwards. With hindsight, the example set by Liang et al., (2007)[82] indicates that varying the alcohol

[a] An alternative solution to this temperature probe issue would have been to purchase another thermocouple, attach a ferrule higher up, and simply bend the thermocouple as appropriate to reach the bottom of the reaction chamber).

used in this hybrid solvothermal synthesis from ethanol to methanol may have produced the cube-shaped UCNPs produced by Bi et al., (2022).[106] We also did not explore many variables, such as precursor choice, ratio of various reactants, pH, and ratio of solvents such as OA and ODE. With such a large parameter space to explore, parallel batch synthesis of UCNPs (e.g. via multi-chamber autoclaves or simultaneously heating many autoclaves at once via oven or heat-block) would have been highly advantageous in order to increase research efficiency.

2.3.4. Case study #2: solvothermal autoclave synthesis of water-dispersible PEI-UCNPs

As a contrasting case study, we present a solvothermal autoclave synthesis method for producing PEI-coated UCNPs. We adapted this solvothermal method from both Zhang et al., (2014)[116] and Nampi et al., (2018)[62] and have found it to be particularly reliable. In brief, rare earth nitrate hydrates, NaCl, and PEI polymer (branched PEI, average molecular weight 25,000) are all dissolved and mixed in ethylene glycol. This is combined with NH_4F in ethylene glycol and then transferred to an autoclave. In this procedure, the only sources of water are incidental: arising from the rare earth nitrate hydrate starting materials and the humidity ambient atmosphere (either via direct exposure and/or due to the hygroscopic nature of ethylene glycol and various other starting materials). Further, ethylene glycol is miscible with water, therefore even if water is present, no micelles are expected to be formed and this may be considered a purely solvothermal autoclave synthesis. Zhang et al., do not detail the autoclave used, whereas Nampi et al., state they used a Parr Pressure Instrument Company autoclave (albeit an unspecified model) with a volume of 120 mL and PTFE liner. Both Zhang et al., and Nampi et al., state that the autoclave is heated at 200 °C for 2 hours, but do not state the style of autoclave or how it was heated. We have found that following published protocols in our Asynt PressureSyn autoclave reactor reliably produces PEI-UCNPs with properties (i.e. size, crystal structure, and luminescence) that closely match prior studies (see Figure 8a). For example, our powder x-ray diffraction studies have measured an alpha-phase crystal lattice parameter of 5.47 ± 0.01 Å, which is consistent with the value of 5.47 ± 0.02 Å reported by Nampi et al. Notably, the UCNPs are fairly small (~16 ± 3 nm) with a large hydrodynamic diameter 148 ± 65 nm (measured by dynamic light scattering) and strong positive zeta potential (typically +28 mV) indicating that the PEI polymer enables the PEI-UCNPs to be well dispersed in water. Furthermore, the $NaYF_4$:Yb,Er UCNPs (Yb = 18 mol%, Er = 2 mol %) produced exhibit remarkable unusually strong red emission for $NaYF_4$:Yb,Er UCNPs without Mn^{2+} co-doping; this may indicate that the PEI is protecting the $^4F_{9/2} \rightarrow {}^4I_{15/2}$ emission pathway or Er^{3+} ions. We have observed that strong acid treatment of these PEI-UCNPs at least partially strips away the protective PEI and results in a loss of their luminescence, which we ascribe to upconversion luminescence quenching in water.[17]

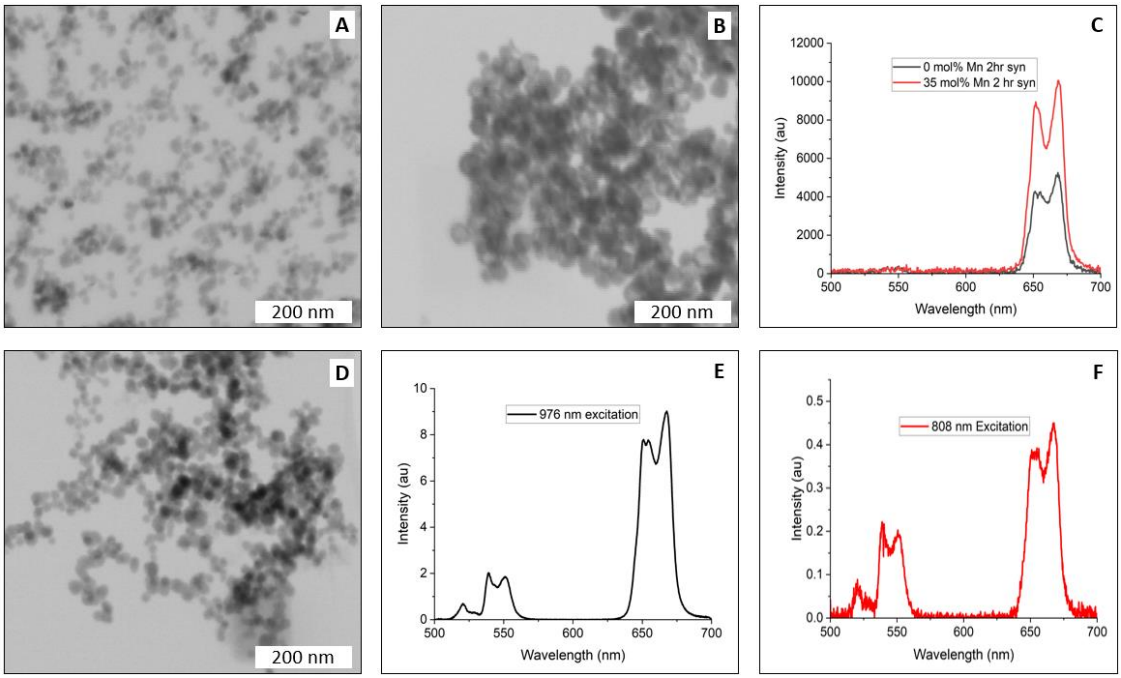

Figure 8. PEI-UCNPs produced as per described in Case Study #2. (A) STEM image of $NaYF_4$:Yb,Er PEI UCNPs (Yb = 18 mol %, Er = 2 mol %). (B) STEM images of $NaYF_4$:Yb,Er,Mn UCNPs (Yb = 18 mol %, Er = 2 mol %, Mn = 35 mol %) exhibiting potentially hollow structures. (C) Upconversion emission spectra of these UCNPs at 10 mg/mL in deionised water under 976 nm excitation.[b] (D) STEM image of $NaYF_4$:Yb,Er@$NaYF_4$:Yb,Nd core/shell PEI UCNPs. (E) Emission of 1.5 mg/mL $NaYF_4$:Yb,Er@$NaYF_4$:Yb,Nd core/shell PEI UCNPs (core: Yb^{3+} 20 mol %, Er^{3+} 2 mol %; shell core: Yb^{3+} 20 mol %, Nd^{3+} 10 mol %) dispersed in water and excited at 976 nm. (F) Emission of same UCNPs as (E), excited at 808 nm.[c]

In a small exploratory study, we introduced Mn^{2+} co-doping (Yb^{3+} = 18 mol %, Er^{3+} = 2 mol %, Mn^{2+} = 35 mol %) into PEI-UCNP synthesis with the aim of increasing red emission in a manner similar to our prior work with PVP-UCNPs (i.e. via constricting unit cell diameter and enabling a three-photon sensitization pathway).[10] As expected, we found that 35 mol% Mn^{2+} co-doping increased PEI-UCNP red band emission by approximately a factor of 3 over standard $NaYF_4$:Yb,Er PEI UCNPs (see Figure 8c). However, electron microscopy revealed that the Mn^{2+} co-doped PEI-UCNPs were not uniform in nature, rather they appeared to be hollow and larger than PEI-UCNPs without Mn^{2+} (see Figure 8a,b). These initial results may indicate that Mn^{2+} may bind to PEI in a way that alters resulting PEI-UCNP morphology; this may be consistent with the less-regular UCNPs observed when Mn^{2+} is used in co-doping in synthesis of PVP-UCNPs,[10] and hollow cubic-shaped OA-UCNPs.[117,118] Further study is required to investigate such effects.

Despite the advantage of immediate water dispersibility inherent to PEI-UCNPs, the number of papers published for PEI-UCNP synthesis seems to be considerably less than OA-UCNPs. A variety of dopant combinations have been explored for PEI-UCNPs to produce various emission colours, including Tm^{3+}

[b] These spectra were measured on a relatively low-cost modular upconversion spectrometer system consisting of a 900 mW 976 nm laser (BL976-PAG900 mounted on a CLD1015, Thorlabs), fibre optic delivery and collimating lens, a sample holder, short-pass filter (< 700 nm) fibre optic output, and a CCD spectrometer (OCEAN-HDXXR, Ocean Insight). This low-cost upconversion spectrometer has a poorer signal to noise ratio than well optimised upconversion spectrometers. Additionally, spurious CCD artefacts as can be seen at ~740 nm in Figure 8C.

[c] Measured with the upconversion spectroscopy system previously reported in Birch et al., (2023).[2]

to achieve higher-energy blue PEI-UCNP emission.[119–121,121] Some notable examples include use of Gd to achieve green emission,[122,123] achieving red and green emission by varying ratio of Yb^{3+} to Er^{3+},[124] and achieving both red and blue emission by varying ratio of Yb^{3+} to Tm^{3+}.[124] Intriguingly, Hu et al., (2014) [125] demonstrated that simply varying the amount of water in the solvothermal PEI-UCNP synthesis can select for production of cubic-phase PEI-$NaYF_4$;Yb,Er UCNPs (strong red emission) or hexagonal-phase PEI-$NaYF_4$;Yb,Er UCNPs (strong green emission) via reaction in a 25 mL PTFE-lined autoclave at 200 °C for 10 hours.[125] Some studies have formed silica shells around PEI-UCNPs, but to the best of our knowledge, mesoporous silica shells have not yet been formed around PEI-UCNPs.[123]

In another exploratory study, we adapted the PEI-UCNP methodology to enable dual-wavelength 808 nm and 976 nm excitation by adding a Nd^{3+} doped shell to the PEI-UCNPs. The resulting $NaYF_4$:Yb,Er@$NaYF_4$:Yb,Nd core/shell PEI UCNPs are shown in Figure 8D with corresponding emission spectra in Figure 8E and Figure 8F. This initial data is promising, but further well-resourced study is required to optimize these UCNPs, examine dopant distribution and shell formation, and to fully characterize their photophysical properties. Nevertheless, PEI-UCNPs appear to be a rather straight-forward route to small-diameter water-dispersible UCNPs with multi-wavelength capabilities.

Whilst the reliability of PEI-UCNP synthesis is favorable, we have noticed one issue which results in failed synthesis: over-hydrated/wet hygroscopic staring reagents. Being situated in Scotland, our laboratory is a high-humidity environment, therefore various hygroscopic reagents used in the synthesis (i.e. rare earth nitrate hydrates, ammonium fluoride, and ethylene glycol) will absorb atmospheric water. This will change the carefully balanced stoichiometry of input materials over time, which manifests as a gradual reduction of UCNP emission intensity, eventually leading to optically-inert nanoparticle formation. Our solution to this is simply to periodically purchase fresh reagents.

In summary, PEI-UCNPs offer a reliable route to water-dispersible UCNPs that seem particularly favourable for biophotonic applications. For example, a number of studies have demonstrated that PEI-UCNPs have good biocompatibility and can be taken up by cells and tissues.[62,64,66] Jin et al., (2011) established that PEI-UCNPs are taken up via a clathrin endocytic mechanism.[64] Further, the highly positively charged PEI itself could be exploited to bind various molecules and proteins non-specifically (by simple electrostatic interactions) or specifically (by rationale-controlled organic modification of the PEI polymer). Overall, PEI-UCNP seems to be a highly reliable method of producing water dispersible UCNPs via solvothermal autoclave reactions and there is plenty of scope for future studies to push the boundaries of what is possible for PEI-UCNPs.

2.4. Discussion of non-autoclave UCNP synthesis techniques

2.4.1. Microwave synthesis of UCNPs

Microwave synthesis of UCNPs is less well established than autoclave synthesis or hot-injection methods, yet it is highly attractive because contemporary microwave reactors offers straight-forward operation, excellent control of synthesis variables, and short reaction times (e.g. 1 second to 10 minutes for enclosed reactors with pressurised vessels).[126] In microwave UCNP synthesis, the reaction mixture is contained in reinforced closed reaction vessels capable of withstanding elevated temperatures and pressures to similar tolerances of autoclaves. For example, some MARS 6 (CEM Corporation) reaction vessels can reportedly handle pressures of up to 55 bar at 240 °C or 7 bar at 300 °C.[127] In larger bench-top microwave, multiple reaction vessels are often housed in a rotating carousel, allowing parallel batch synthesis of UCNPs in a convenient manner. Heating is induced via microwave dielectric heating of the reaction mixture – which requires careful consideration, especially where there is little to no water in reactions.[128] Contemporary microwave reactors will offer in-line

temperature monitoring and data reporting, which is highly beneficial for reproducibility - see the recently reported example by Egatz-Gomez et al.[129] Some microwave reactors may even enable visual monitoring of the reaction mixture via camera systems. Stirring is possible via magnetic systems. Further, they may enable addition of pressurised gas and use of autosamplers. Reaction times can be as short as 10 minutes. Ultimately the potential for batch production of UCNPs in minutes at the push of a button, makes microwave UCNP synthesis highly desirable in both research and industrial production settings.

Arguably, the only current downsides to microwave synthesis of UCNPs are that: (a) microwave synthesis is somewhat less well established in terms of the body of the literature, and (b) microwave equipment may be more costly than equipment required for autoclave and hot-injection method (although syringe-pumps for hot injection can be highly expensive). That said, in our recent enquiries, small single-chamber microwave reactors are comparable in price to single-chamber high-safety autoclave systems.

Yet there are some unique variables to consider in microwave synthesis of UCNPs. For example, choice of solvent plays a crucial role in how products are heated. Polar solvents (e.g. water, ethylene glycol, benzyl alcohol) are heated efficiently due to these solvents offering good microwave absorption; however, these generally produce larger nanoparticles. OA/ODE mixtures absorb microwaves less efficiently, but produce smaller nanoparticles.[128] Examples of solvents used in microwave UCNP synthesis include aqueous solutions[130,131] ; mixtures of OA, ODE, olamine (OAm)[109]; and bis(2-ethylhexyl) adipate (BEHA).[129] As an aside, recently gum Arabic has been used to render OA-capped microwave synthesised UCNPs water dispersible via emulsification; a convenient procedure for printing UCNP security inks using commercial jet printers.[132] Notably, UCNP precursor selection may also vary the heating rate achieved.[128] It is also known that different precursors (e.g. $[Ln(TFA)_3]$, $[Ln(OA)_3]$, $[Ln(Ac)_3]$), thermally decompose at different temperatures, resulting in nucleation of UCNPs at different temperatures, altered pressure during the course of UCNP synthesis, and ultimately differences in final UCNP size.[109] Some examples of UCNPs produced by microwave synthesis include: sub 5 nm $Na(Gd\text{-}Yb)F_4$:Tm UCNPs [128]; sub-10 nm core/shell β-phase $NaGdF_4$:Yb,Er UCNPs (reaction time between 1 second to 10 minutes)[109]; microparticles with upconversion and downshifting capabilities ($LiYbF_4$, $NaYF_4$, $NaGdF_4$, $LiYF_4$ host lattices with various emissive dopants, i.e. Yb^{3+},Er^{3+} – Yb^{3+},Tm^{3+} – Ce^{3+},Tm^{3+})[130]; $NaYF_4$:Yb/Er with subsequent mesoporous silica coating[131]; LaOF:Yb^{3+},Ho^{3+} UCNP nanorods[133]; and rhombus-shaped GdF_3:Yb,Er UCNPs.[134]

Aside from UCNP synthesis, microwave reactors are often used for digestion of both organic and inorganic samples via acid treatment.[135,136] Reputable manufacturers of microwave reactors include Anton Parr GmBH (Germany) and CEM Corporation (NC, USA).

Overall, microwave synthesis of UCNPs produces high-quality UCNPs in a highly controlled manner on a short timescale, with ample opportunity for parallel synthesis in multiple reaction vessels. Microwave reactions require careful experimental design to achieve desired synthesis results but there is an expanding body of literature on suitable methods. Like autoclave synthesis, key variables such as reactor and reaction chambers used should be reported for microwave synthesis techniques to be reproducible. Ultimately, microwave UCNP synthesis is highly attractive UCNP synthesis route.

2.4.2. Hot-injection/Thermal Co-Precipitation synthesis

Hot-injection (also known as “thermal co-precipitation”) is the UCNP synthesis that offers the most control over form and quality of UCNPs produced albeit at the requirement of a high-degree of operator skill. For example, it can be used to make extraordinarily sophisticated $NaErF_4$:Tm core/multi-

shell UCNPs with various six-shell layers,[6] small and bright UV-emissive $LiYbF_4$:Tm@$LiYF_4$ core/multi-shell UCNPs,[8] and $NaYF_4$:Yb,Er, @$NaYF_4$ core/shell UCNPs with record-breaking quantum yields.[35]

The hot-injection method is demanding. It requires multiple three necked round bottom flasks, a gas control system (e.g. a Schlenk line), one or multiple syringe pumps, heating mantles, and a skilled operator experienced enough to work with all these elements safely. As a general example of this synthesis method, rare-earth salts are dissolved in a mixture of water and acid to form precursors. These precursors are then introduced OA in a separate reaction flask under vacuum or inert atmosphere, which is then heated at elevated temperature (e.g. 100 – 120 °C) to form rare-earth oleates. In the next step, the missing fluoride source and Na^+ or Li^+ source (depending on desired host lattice nanomaterial) are added to the oleates, and after another cycle of degassing and dissolving, the hot solution is transferred to a heated syringe and injected into a pre-degassed mix high boiling-point solvents at elevated temperature (e.g. OA/ODE/OAm at 300 – 360°C). This reaction mixture is kept at the elevated temperature for several hours, with precursors decomposing to form the core UCNPs. The core UCNPs are then collected via centrifugation and washed. Subsequent layers of shells are formed around UCNPs by repeating similar reactions with UCNPs present and injecting new precursor materials. [8,137]

There are a number of variables to consider in hot-injection synthesis. For example, OAm can be incorporated as a less strongly coordinating solvent, and ODE can be used as a non-coordinating solvent; altering the ratio of OA, OAm, and ODE will alter the morphology of UCNPs produced.[8] Likewise, the precursor, their ratios, addition rates, and water content can all affect morphology and properties of the resultant UCNPs. Production of the highest-performance UCNPs requires diligent choice of precursors, dry (i.e. water-free) solvents, and a sophisticated approach wherein precursor cubic-phase UCNPs were redissolved in fresh solvent to obtain hexagonal-phase UCNPs.[35] However, given that the reaction occurs in a single flask, hot-injection UCNP synthesis is poorly suited to iteratively exploring the parameter space of UCNP composition.

Andresen et al., (2023)[138] have produced a detailed study of the reproducibility of UCNPs produced by the hot-injection method at various scales. They found that despite the complexity of mass transport dynamics and seed nanocrystal formation, the hot-injection reaction could be upscaled to 5 g per batch. You et al., (2018)[139] also demonstrated a hot-injection synthesis of beta-phase core/shell UCNPs at over 60 g per batch.[139] Therefore, despite its complexities, hot-injection UCNP synthesis is attractive for large-batch production of UCNPs.

Ultimately, the hot-injection UCNP synthesis method may be viewed as the highest-performance UCNP synthesis technique because it enables production of exceptional quality core/shell UCNP products. However, it requires highly skilled personnel with a strong chemistry background to control all the variables involved and to undertake air and water-free reactions safely and, more fundamentally, only a single reaction can be undertaken at a time with typical apparatus.

2.5.2. Automated UCNP synthesis, machine-learning, and self-driving fluidic labs

It is worth noting that if cost is not a limiting factor, fully-automated approaches to UCNP synthesis have been demonstrated.[7,14,23,140,141] These approaches require custom-designed robots with the ability to weigh compounds, mix liquids, and heat many vials at once up to 325 °C in oxygen-free environments.[142] Such automated systems massively reduce time to results where many variables are involved. For example, the screening of 78 UCNP dopants combinations (as demonstrated in Chan et al., (2012)[7]) would require around 4 months of continuous synthesis work with a standard single-chamber autoclave reactor (assuming one synthesis cycle per day due to heat-up/cool-down times), but would likely take less than a single day to achieve with an automated nanomaterial synthesis

system. This time advantage of automated nanomaterial synthesis laboratories enables exploration of sophisticated nanoarchitectures.

At the time of writing in 2024, we are experiencing a nascent epoch of machine learning approaches being applied to scientific challenges, with nanoparticle engineering being no exception. Recently, Xia et al., (2023)[143] reported machine learning-driven approaches have recently been reported to theoretically optimise multi-shell UCNP composition and architecture via simulation.[143] On the practical side of nanomaterial synthesis, Bateni et al., (2024)[144] reported that a closed-loop "self driving fluidic lab" produced record breaking Mn-Yb co-doped $CsPbCl_3$ quantum dots with a photoluminescence quantum yield of 158%.[144] Such approaches have huge advantages not only in quality of output products, but also in terms of material cost and labour time. Given that the self-driving fluidic lab incorporates atmospheric control, pressure containment, and high-temperature synthesis, it seems likely that it will only be a matter of time before such self-driving fluidic lab approaches are turned to the production of UCNPs.

3. Conclusion and outlook

Upconversion nanomaterials have emerged and flourished in the past two decades with multiple UCNP synthesis techniques emerging. Consequently, navigating both the basic requirements and chemical intricacies of UCNP synthesis can be daunting and time-consuming for those new to the field. In particular, because the basic workings of a UCNP synthesis and how this interplays with equipment and reaction conditions are often not discussed or reported in the literature.

Despite a large number of publications reporting the use of autoclaves for synthesis of UCNPs, the basic details and operation of autoclave equipment remains generally unreported. This stymied reproducibility of published synthesis methods. We have provided two case studies in which we adapted autoclave-assisted UCNP protocols from the literature for use with a high-safety autoclave reactor. Additionally, we have recommended that a large number of autoclave variables should be reported in synthesis (see Table 1). We hope these case studies and recommendations will be beneficial to others looking to adapt autoclave synthesis in similar manners.

We note that there are various regulations and legalities covering the use of autoclaves in for research and work purposes. We also note that a number of high-safety autoclave reactors are now available from reputable manufacturers, and highlight advantages in terms of reducibility, safety, and experimental control that such systems may provide. We recommend that only autoclaves made by reputable manufacturers and which are certified/tested to comply with appropriate international regulatory standards should be used in the synthesis of UCNPs and other nanomaterials.

References

1. Mackenzie, L. E. *et al.* The theoretical molecular weight of NaYF4:RE upconversion nanoparticles. *Scientific Reports* **8**, 1106 (2018).
2. Birch, R. *et al.* Influence of polyvinylpyrrolidone (PVP) in the synthesis of luminescent NaYF4:Yb,Er upconversion nanoparticles. *Methods Appl. Fluoresc.* **11**, 034001 (2023).
3. Bünzli, J.-C. G. & Eliseeva, S. V. Basics of Lanthanide Photophysics. in *Lanthanide Luminescence* (eds. Hänninen, P. & Härmä, H.) vol. 7 1–45 (Springer Berlin Heidelberg, Berlin, Heidelberg, 2010).
4. Auzel, F. History of upconversion discovery and its evolution. *Journal of Luminescence* **223**, 116900 (2020).
5. Jurga, N., Ryszczyńska, S. & Grzyb, T. Designing photon upconversion nanoparticles capable of intense emission in whole human blood. *Spectrochimica Acta Part A: Molecular and Biomolecular Spectroscopy* **303**, 123220 (2023).
6. Mun, K. R. *et al.* Elemental-Migration-Assisted Full-Color-Tunable Upconversion Nanoparticles for Video-Rate Three-Dimensional Volumetric Displays. *Nano Lett.* (2023) doi:10.1021/acs.nanolett.3c00397.
7. Chan, E. M. *et al.* Combinatorial discovery of lanthanide-doped nanocrystals with spectrally pure upconverted emission. *Nano Letters* **12**, 3839–3845 (2012).
8. Cheng, T., Marin, R., Skripka, A. & Vetrone, F. Small and Bright Lithium-Based Upconverting Nanoparticles. *J. Am. Chem. Soc.* **140**, 12890–12899 (2018).
9. Mironova, K. E. *et al.* Ultraviolet phototoxicity of upconversion nanoparticles illuminated with near-infrared light. *Nanoscale* **9**, 14921 (2017).
10. Mackenzie, L. E., Alvarez-ruiz, D. & Pal, R. Low-temperature open-air synthesis of PVP-coated NaYF 4 : Yb , Er , Mn upconversion nanoparticles with strong red emission. *Royal Society Open Science* **9**, 211508 (2022).

11. Tang, J. *et al.* Selectively enhanced red upconversion luminescence and phase/size manipulation via Fe3+ doping in NaYF4:Yb,Er nanocrystals. *Nanoscale* **7**, 14752–14759 (2015).
12. Tian, G. *et al.* Mn2+ dopant-controlled synthesis of NaYF4:Yb/Er upconversion nanoparticles for in vivo imaging and drug delivery. *Advanced Materials* **24**, 1226–1231 (2012).
13. Moghadam, R. Z., Dizagi, H. R., Agren, H. & Ehsani, M. H. Understanding the effect of Mn2+ on Yb3+/Er3+ co-doped NaYF4 upconversion and obtaining the optimal combination of these tridoping. *Sci Rep* **13**, 17556 (2023).
14. Zhao, Z. *et al.* Multifunctional Core–Shell Upconverting Nanoparticles for Imaging and Photodynamic Therapy of Liver Cancer Cells. *Chemistry – An Asian Journal* **7**, 830–837 (2012).
15. Liu, N. *et al.* Core–multi-shell design: unlocking multimodal capabilities in lanthanide-based nanoparticles as upconverting, T2-weighted MRI and CT probes. *Nanoscale* **15**, 19546–19556 (2023).
16. Sun, Y. *et al.* Fluorine-18 labeled rare-earth nanoparticles for positron emission tomography (PET) imaging of sentinel lymph node. *Biomaterials* **32**, 2999–3007 (2011).
17. Arppe, R. *et al.* Quenching of the upconversion luminescence of NaYF 4 :Yb 3+ , Er 3+ and NaYF 4 :Yb 3+ , Tm 3+ nanophosphors by water: the role of the sensitizer Yb 3+ in non-radiative relaxation. *Nanoscale* **7**, 11746–11757 (2015).
18. Przybylska, D. & Grzyb, T. Synthesis and up-conversion of core/shell SrF2:Yb3+,Er3+@SrF2:Yb3+,Nd3+ nanoparticles under 808, 975, and 1532 nm excitation wavelengths. *Journal of Alloys and Compounds* **831**, 154797 (2020).
19. Demchenko, A. P. Photobleaching of organic fluorophores: quantitative characterization, mechanisms, protection*. *Methods Appl. Fluoresc.* **8**, 022001 (2020).
20. Shi, X., Tu, Y., Liu, X., Yeung, E. S. & Gai, H. Photobleaching of quantum dots by non-resonant light. *Phys. Chem. Chem. Phys.* **15**, 3130–3132 (2013).
21. Efros, A. L. & Nesbitt, D. J. Origin and control of blinking in quantum dots. *Nature Nanotech* **11**, 661–671 (2016).

22. Linde, S. van de & Sauer, M. How to switch a fluorophore: from undesired blinking to controlled photoswitching. *Chem. Soc. Rev.* **43**, 1076–1087 (2014).

23. Ostrowski, A. D. *et al.* Controlled Synthesis and Single-Particle Imaging of Bright, Sub-10 nm Lanthanide-Doped Upconverting Nanocrystals. *ACS Nano* **6**, 2686–2692 (2012).

24. Lu, D. *et al.* Nanojet Trapping of a Single Sub-10 nm Upconverting Nanoparticle in the Full Liquid Water Temperature Range. *Small* **17**, 2006764 (2021).

25. McLellan, C. A. *et al.* Engineering Bright and Mechanosensitive Alkaline-Earth Rare-Earth Upconverting Nanoparticles. *J. Phys. Chem. Lett.* **13**, 1547–1553 (2022).

26. Fardian-Melamed, N. *et al.* Infrared nanosensors of pico- to micro-newton forces. Preprint at https://doi.org/10.48550/arXiv.2404.02026 (2024).

27. Hong, A.-R., Kyhm, J.-H., Kang, G. & Jang, H. S. Orthogonal R/G/B Upconversion Luminescence-based Full-Color Tunable Upconversion Nanophosphors for Transparent Displays. *Nano Lett.* **21**, 4838–4844 (2021).

28. Arppe, R. & Sørensen, T. J. Physical unclonable functions generated through chemical methods for anti-counterfeiting. *Nature Reviews Chemistry* **1**, 0031 (2017).

29. Mackenzie, L. E. & Pal, R. Circularly polarized lanthanide luminescence for advanced security inks. *Nature Reviews Chemistry* (2020) doi:10.1038/s41570-020-00235-4.

30. Meruga, J. M. *et al.* Stable Inks Containing Upconverting Nanoparticles Based on an Oil-in-Water Nanoemulsion. *Langmuir* **34**, 1535–1541 (2018).

31. Xu, X. *et al.* Dual-functional α-NaYb(Mn)F4:Er3+@NaLuF4 nanocrystals with highly enhanced red upconversion luminescence. *RSC Advances* **6**, 33493–33500 (2016).

32. Park, H. S. *et al.* Clear-cut observation of clearance of sustainable upconverting nanoparticles from lymphatic system of small living mice. *Scientific Reports* **6**, 1–7 (2016).

33. Jacques, S. L. Optical properties of biological tissues: a review. *Physics in medicine and biology* **58**, R37-61 (2013).

34. Chen, G. *et al.* Advanced Near-Infrared Light for Monitoring and Modulating the Spatiotemporal Dynamics of Cell Functions in Living Systems. *Advanced Science* **7**, 1903783 (2020).

35. Homann, C. *et al.* NaYF4:Yb,Er/NaYF4 Core/Shell Nanocrystals with High Upconversion Luminescence Quantum Yield. *Angewandte Chemie International Edition* **57**, 8765–8769 (2018).

36. Quintanilla, M. *et al.* Cubic versus Hexagonal – Phase, Size and Morphology Effects on the Photoluminescence Quantum Yield of NaGdF 4 :Er 3+ /Yb3+ Upconverting Nanoparticles. *Nanoscale* (2022) doi:10.1039/d1nr06319g.

37. Grabolle, M. *et al.* Determination of the Fluorescence Quantum Yield of Quantum Dots: Suitable Procedures and Achievable Uncertainties. *Anal. Chem.* **81**, 6285–6294 (2009).

38. Shim, H. S. *et al.* InP/ZnSeS/ZnS Quantum Dots with High Quantum Yield and Color Purity for Display Devices. *ACS Appl. Nano Mater.* **6**, 1285–1294 (2023).

39. Hu, X. *et al.* Naked eye detection of multiple tumor-related mRNAs from patients with photonic-crystal micropattern supported dual-modal upconversion bioprobes. *Chemical Science* **8**, 466–472 (2017).

40. Li, D., Lai, W.-Y., Shen, X., Shao, Q. & Huang, W. Real-time naked-eye recognizable temperature monitoring based on Ho 3+ (or Tm 3+)-activated NaYF 4 upconversion nanowires via visual multicolor alteration. *Materials Chemistry Frontiers* **3**, 791–795 (2019).

41. Wu, X. *et al.* Tailoring dye-sensitized upconversion nanoparticle excitation bands towards excitation wavelength selective imaging. *Nanoscale* **7**, 18424–18428 (2015).

42. Muhr, V. *et al.* Particle-Size-Dependent Förster Resonance Energy Transfer from Upconversion Nanoparticles to Organic Dyes. *Analytical Chemistry* **89**, 4868/4874 (2017).

43. Pini, F., Francés-Soriano, L., Andrigo, V., Natile, M. M. & Hildebrandt, N. Optimizing Upconversion Nanoparticles for FRET Biosensing. *ACS Nano* **17**, 4971–4984 (2023).

44. Lee, J. *et al.* Ultra-Wideband Multi-Dye-Sensitized Upconverting Nanoparticles for Information Security Application. *Advanced Materials* **29**, 1603169 (2017).

45. Wang, X. *et al.* Triplet-Induced Singlet Oxygen Photobleaches Near-Infrared Dye-Sensitized Upconversion Nanosystems. *Nano Lett.* **23**, 7001–7007 (2023).

46. Kaur, M., Mandl, G. A., Maurizio, S. L., Tessitore, G. & Capobianco, J. A. On the photostability and luminescence of dye-sensitized upconverting nanoparticles using modified IR820 dyes. *Nanoscale Advances* 608–618 (2022) doi:10.1039/d1na00710f.

47. Wang, M., Wei, H., Wang, S., Hu, C. & Su, Q. Dye Sensitization for Ultraviolet Upconversion Enhancement. *Nanomaterials* **11**, 3114 (2021).

48. Zou, W., Visser, C., Maduro, J. A., Pshenichnikov, M. S. & Hummelen, J. C. Broadband dye-sensitized upconversion of near-infrared light. *Nature Photonics* **6**, 560–564 (2012).

49. Wang, X. *et al.* Dye-sensitized lanthanide-doped upconversion nanoparticles. *Chem. Soc. Rev.* **46**, 4150–4167 (2017).

50. Yin, D. *et al.* Huge enhancement of upconversion luminescence by broadband dye sensitization of core/shell nanocrystals. *Dalton Transactions* **45**, 13392–13398 (2016).

51. Energy-Cascaded Upconversion in an Organic Dye-Sensitized Core/Shell Fluoride Nanocrystal | Nano Letters. https://pubs.acs.org/doi/10.1021/acs.nanolett.5b02830.

52. Liu, Xiaomeng., Liu, T., Feng, Y. & Yao, C.-J. Toward Upconversion Luminescence Enhancement with Dye Sensitization. *ACS Appl. Opt. Mater.* (2023) doi:10.1021/acsaom.3c00194.

53. Liu, T., Liu, X., Feng, Y. & Yao, C.-J. Advances in plasmonic enhanced luminenscence of upconversion nanoparticles. *Materials Today Chemistry* **34**, 101788 (2023).

54. Zhang, F. *et al.* Brownian Motion Governs the Plasmonic Enhancement of Colloidal Upconverting Nanoparticles. *Nano Lett.* **24**, 3785–3792 (2024).

55. Ouyang, Y.-C., Yeom, B.-J., Zhao, Y. & Ma, W. Progress and prospects of chiral nanomaterials for biosensing platforms. *Rare Met.* (2024) doi:10.1007/s12598-023-02602-8.

56. Khan, I. M., Niazi, S., Mohsin, A. & Zhou, Y. Soft scaffold aided plasmon-enhanced upconversion luminescence and its application in vascular endothelial growth factor (VEGF) detection. *Sensors and Actuators B: Chemical* **410**, 135657 (2024).

57. Mackenzie, L. & Parker, D. Circularly polarised luminescence laser scanning confocal microscopy to study live cell chiral molecular interactions. 1–8 doi:10.1038/s41467-022-28220-z.

58. Cao, T. *et al.* Water-soluble NaYF4:Yb/Er upconversion nanophosphors: Synthesis, characteristics and application in bioimaging. *Inorganic Chemistry Communications* **13**, 392–394 (2010).

59. Quintanilla, M., X. Cantarelli, I., Pedroni, M., Speghini, A. & Vetrone, F. Intense ultraviolet upconversion in water dispersible SrF 2 :Tm 3+ ,Yb 3+ nanoparticles: the effect of the environment on light emissions. *Journal of Materials Chemistry C* **3**, 3108–3113 (2015).

60. Cao, T. *et al.* Biodistribution of sub-10 nm PEG-modified radioactive/upconversion nanoparticles. *Biomaterials* **34**, 7127–7134 (2013).

61. Zhang, X., Zhang, W., Zhang, X. & Wang, Y. Facile Fabrication of Upconversion Photoluminescent Transparent Semiaromatic Polyamide Nanocomposites Through Interfacial Chemistry Modification. *ACS Omega* **5**, 29838–29843 (2020).

62. Nampi, P. P. *et al.* Selective cellular imaging with lanthanide based upconversion nanoparticles. *Journal of Biophotonics* e201800256 (2018) doi:10.1002/jbio.201800256.

63. Li, Z. & Zhang, Y. Monodisperse silica-coated polyvinyl-pyrrolidone/NaYF4 nanocrystals with multicolor upconversion fluorescence emission. *Angewandte Chemie - International Edition* **45**, 7732–7735 (2006).

64. Jin, J. *et al.* Polymer-Coated NaYF4:Yb3+, Er3+ Upconversion Nanoparticles for Charge-Dependent Cellular Imaging. *ACS Nano* **5**, 7838–7847 (2011).

65. Zhang, D. *et al.* The morphology and surface charge-dependent cellular uptake efficiency of upconversion nanostructures revealed by single-particle optical microscopy †. *Chemical Science* **9**, 5260 (2018).

66. Zhong, L. *et al.* Highly Retentive, Anti-Interference, and Covert Individual Marking Taggant with Exceptional Skin Penetration. *Advanced Science* **9**, 2201497 (2022).

67. Zhu, X. *et al.* Large-molecular-weight PVP-functionalized stacked upconversion nanoplates for high-performance individual marking. *Cell Reports Physical Science* **4**, 101572 (2023).

68. Güleryüz, B., Ünal, U. & Gülsoy, M. Near infrared light activated upconversion nanoparticles (UCNP) based photodynamic therapy of prostate cancers: An in vitro study. *Photodiagnosis and Photodynamic Therapy* **36**, 102616 (2021).

69. Fedoryshin, L. L., Tavares, A. J., Petryayeva, E., Doughan, S. & Krull, U. J. Near-Infrared-Triggered Anticancer Drug Release from Upconverting Nanoparticles. *ACS Appl. Mater. Interfaces* **6**, 13600–13606 (2014).

70. Wang, M. *et al.* Immunolabeling and NIR-Excited Fluorescent Imaging of HeLa Cells by Using NaYF4:Yb,Er Upconversion Nanoparticles. *ACS Nano* **3**, 1580–1586 (2009).

71. Li, L.-L., Wu, P., Hwang, K. & Lu, Y. An Exceptionally Simple Strategy for DNA-Functionalized Up-Conversion Nanoparticles as Biocompatible Agents for Nanoassembly, DNA Delivery, and Imaging. *J. Am. Chem. Soc.* **135**, 2411–2414 (2013).

72. Francés-Soriano, L., Estebanez, N., Pérez-Prieto, J. & Hildebrandt, N. DNA-Coated Upconversion Nanoparticles for Sensitive Nucleic Acid FRET Biosensing. *Advanced Functional Materials* **32**, 2201541 (2022).

73. Bhuckory, S. *et al.* Understanding FRET in Upconversion Nanoparticle Nucleic Acid Biosensors. *Nano Lett.* **23**, 2253–2261 (2023).

74. Laurenti, M. *et al.* Enhancement of the Upconversion Emission by Visible-to-Near-Infrared Fluorescent Graphene Quantum Dots for miRNA Detection. *ACS Appl. Mater. Interfaces* **8**, 12644–12651 (2016).

75. Melle, S. *et al.* Förster Resonance Energy Transfer Distance Dependence from Upconverting Nanoparticles to Quantum Dots. *J. Phys. Chem. C* **122**, 18751–18758 (2018).

76. Li, M. *et al.* Red blood cell membrane-coated upconversion nanoparticles for pretargeted multimodality imaging of triple-negative breast cancer. *Biomaterials Science* **8**, 1802–1814 (2020).

77. Zhou, M. *et al.* The Bioavailability, Biodistribution, and Toxic Effects of Silica-Coated Upconversion Nanoparticles in vivo. *Frontiers in Chemistry* **7**, (2019).

78. Shao, B. *et al.* A novel synthetic route towards monodisperse β-NaYF4:Ln3+ micro/nanocrystals from layered rare-earth hydroxides at ultra low temperature. *Chemical Communications* **50**, 12706–12709 (2014).

79. Jiao, Y. *et al.* Controllable Synthesis of Upconversion Nanophosphors toward Scale-Up Productions. *Particle and Particle Systems Characterization* **37**, 1–13 (2020).

80. Lei, P. *et al.* Ultrafast Synthesis of Novel Hexagonal Phase NaBiF4 Upconversion Nanoparticles at Room Temperature. *Advanced Materials* **29**, 4–7 (2017).

81. Du, P., Luo, L., Huang, X. & Yu, J. S. Ultrafast synthesis of bifunctional Er 3+ /Yb 3+ -codoped NaBiF 4 upconverting nanoparticles for nanothermometer and optical heater. *Journal of Colloid and Interface Science* **514**, 172–181 (2018).

82. Liang, X., Wang, X., Zhuang, J., Peng, Q. & Li, Y. Synthesis of NaYF4 Nanocrystals with Predictable Phase and Shape. *Advanced Functional Materials* **17**, 2757–2765 (2007).

83. Lei, P. & Zhang, Y. Hollow upconversion nanoparticles: Synthesis and luminescence in comparison with their solid counterparts. *Chemical Engineering Journal* **426**, 131376 (2021).

84. Bower, J. S., Broughton, G. F. J., Stedman, J. R. & Williams, M. L. A winter NO2 smog episode in the U.K. *Atmospheric Environment* **28**, 461–475 (1994).

85. Stepuk, A., Casola, G., Schumacher, C. M., Krämer, K. W. & Stark, W. J. Purification of NaYF4-Based Upconversion Phosphors. *Chem. Mater.* **26**, 2015–2020 (2014).

86. Li, C., Yang, J., Yang, P., Lian, H. & Lin, J. Hydrothermal Synthesis of Lanthanide Fluorides LnF3 (Ln = La to Lu) Nano-/Microcrystals with Multiform Structures and Morphologies. *Chem. Mater.* **20**, 4317–4326 (2008).

87. Li, J., Wu, Q. & Wu, J. Synthesis of Nanoparticles via Solvothermal and Hydrothermal Methods. in *Handbook of Nanoparticles* (ed. Aliofkhazraei, M.) 1–28 (Springer International Publishing, Cham, 2015). doi:10.1007/978-3-319-13188-7_17-1.

88. Bennett, T. M. *et al.* Clean Block Copolymer Microparticles from Supercritical CO2: Universal Templates for the Facile and Scalable Fabrication of Hierarchical Mesostructured Metal Oxides. *Nano Lett.* **18**, 7560–7569 (2018).

89. Jin, S. *et al.* Catalytic hydrodeoxygenation of anisole as lignin model compound over supported nickel catalysts. *Catalysis Today* **234**, 125–132 (2014).

90. Chandrashekhar, V. G. *et al.* Silica-supported Fe/Fe–O nanoparticles for the catalytic hydrogenation of nitriles to amines in the presence of aluminium additives. *Nat Catal* **5**, 20–29 (2022).

91. Baheti, P. *et al.* Clean synthesis of linear and star amphiphilic poly(ε-caprolactone)-block-poly(ethyl ethylene phosphonate) block copolymers: assessing self-assembly and surface activity. *Green Chem.* **22**, 3248–3261 (2020).

92. Anthony, D. B. *et al.* Crack arrest in finger jointed thermoplastic interleaved CFRC. in *21st International Conference on Composite Materials* (Chinese Society for Composite Materials, 2017).

93. Zhao, Z. *et al.* Extracting tungsten from scheelite concentrate with caustic soda by autoclaving process. *Hydrometallurgy* **108**, 152–156 (2011).

94. Kim, E.-H. *et al.* Single crystal casting of gas turbine blades using superior ceramic core. *Journal of Materials Research and Technology* **9**, 3348–3356 (2020).

95. Fazi, A., Stiller, K., Andrén, H.-O. & Thuvander, M. Cold sprayed Cr-coating on Optimized ZIRLO^{TM} claddings: the Cr/Zr interface and its microstructural and chemical evolution after autoclave corrosion testing. *Journal of Nuclear Materials* **560**, 153505 (2022).

96. PubChem. Ethylene Glycol. https://pubchem.ncbi.nlm.nih.gov/compound/174.

97. PubChem. Oleic Acid. https://pubchem.ncbi.nlm.nih.gov/compound/445639.

98. 1-Octadecene CAS 112-88-9 | 822112. https://www.merckmillipore.com/GB/en/product/1-Octadecene,MDA_CHEM-822112?ReferrerURL=https%3A%2F%2Fwww.google.com%2F.

99. Berghoff GMBH. High-pressure reactors. https://www.berghof-instruments.com/en/products/digestec-dab/.

100. Berghoff GMBH. Metal-free reactors. https://www.berghof-instruments.com/en/products/metal-free-reactors/.

101. Asynt Ltd. PressureSyn – High safety reactor. https://www.asynt.com/product/pressuresyn/.

102. UK Health and Safety Executive. Pressure Systems Safety Regulations 2000 (PSSR). https://www.hse.gov.uk/pressure-systems/pssr.htm.

103. UJK Health and Safety Executive. Health and Safety at Work etc Act 1974 – legislation explained. https://www.hse.gov.uk/legislation/hswa.htm.

104. Lloyds British. The Complete Compliance Manual to Pressure Systems Safety Regulations (PSSR 2000). https://web.archive.org/web/20231020104219/https://www.lloydsbritish.com/pressure-systems-safety-regulations (2023).

105. *Commission Implementing Decision (EU) 2019/1616 of 27 September 2019 on the Harmonised Standards for Pressure Equipment Drafted in Support of Directive 2014/68/EU of the European Parliament and of the Council*. *OJ L* vol. 250 (2019).

106. Bi, S., Deng, Z., Huang, J., Wen, X. & Zeng, S. NIR-II Responsive Upconversion Nanoprobe with Simultaneously Enhanced Single-Band Red Luminescence and Phase/Size Control for Bioimaging and Photodynamic Therapy. *Advanced Materials* **35**, 2207038 (2022).

107. Chia, S. W. & Misran, M. Flow Behavior of Oleic Acid Liposomes in Sucrose Ester Glycolipid Oil-in-Water Emulsions. *J Surfact Deterg* **17**, 1–10 (2014).

108. Zhang, F. *et al.* Uniform Nanostructured Arrays of Sodium Rare-Earth Fluorides for Highly Efficient Multicolor Upconversion Luminescence. *Angewandte Chemie* **119**, 8122–8125 (2007).

109. Halimi, I. *et al.* Pick your precursor! Tailoring the size and crystal phase of microwave-synthesized sub-10 nm upconverting nanoparticles. *Journal of Materials Chemistry C* **7**, 15364–15374 (2019).

110. Mai, H.-X., Zhang, Y.-W., Sun, L.-D. & Yan, C.-H. Size- and Phase-Controlled Synthesis of Monodisperse NaYF4:Yb,Er Nanocrystals from a Unique Delayed Nucleation Pathway Monitored with Upconversion Spectroscopy. *J. Phys. Chem. C* **111**, 13730–13739 (2007).

111. Liu, C. & Chen, D. Controlled synthesis of hexagon shaped lanthanide-doped LaF3 nanoplates with multicolor upconversion fluorescence. *J. Mater. Chem.* **17**, 3875–3880 (2007).

112. Sui, Y., Tao, K., Tian, Q. & Sun, K. Interaction Between Y3+ and Oleate Ions for the Cubic-to-Hexagonal Phase Transformation of NaYF4 Nanocrystals. *J. Phys. Chem. C* **116**, 1732–1739 (2012).

113. Ding, M., Lu, C., Cao, L., Ni, Y. & Xu, Z. Controllable synthesis, formation mechanism and upconversion luminescence of β-NaYF4:Yb3+/Er3+ microcrystals by hydrothermal process. *CrystEngComm* **15**, 8366–8373 (2013).

114. Li, C. *et al.* Different Microstructures of β-NaYF4 Fabricated by Hydrothermal Process: Effects of pH Values and Fluoride Sources. *Chem. Mater.* **19**, 4933–4942 (2007).

115. Mai, H.-X. *et al.* High-Quality Sodium Rare-Earth Fluoride Nanocrystals: Controlled Synthesis and Optical Properties. *J. Am. Chem. Soc.* **128**, 6426–6436 (2006).

116. Zhang, S. *et al.* Fluorescence resonance energy transfer between NaYF4:Yb,Tm upconversion nanoparticles and gold nanorods: Near-infrared responsive biosensor for streptavidin. *Journal of Luminescence* **147**, 278–283 (2014).

117. Liu, Y. *et al.* Single band red emission of Er3+ ions heavily doped upconversion nanoparticles realized by active-core/active-shell structure. *Ceramics International* (2021) doi:10.1016/j.ceramint.2021.03.220.

118. Liu, Y. *et al.* Highly efficient upconversion single red emission of hollow cubic α-NaErF4 nanoparticles by Mn/Yb heavy doping. *Journal of Luminescence* **228**, 117637 (2020).

119. Xu, S. *et al.* A novel upconversion, fluorescence resonance energy transfer biosensor (FRET) for sensitive detection of lead ions in human serum. *Nanoscale* **6**, 12573–12579 (2014).

120. Zhang, D. *et al.* Mitochondrial specific photodynamic therapy by rare-earth nanoparticles mediated near-infrared graphene quantum dots. *Biomaterials* **153**, 14–26 (2018).

121. Liu, J. *et al.* Up-conversion fluorescence biosensor for sensitive detection of CA-125 tumor markers. *Journal of Rare Earths* **37**, 943–948 (2019).

122. Liu, R. *et al.* Development of a fluorescence aptasensor for rapid and sensitive detection of Listeria monocytogenes in food. *Food Control* **122**, 107808 (2021).

123. Ding, C. *et al.* Ratiometric Upconversion Luminescence Nanoprobe with Near-Infrared Ag2S Nanodots as the Energy Acceptor for Sensing and Imaging of pH in Vivo. *Anal. Chem.* **91**, 7181–7188 (2019).

124. Li, X. *et al.* New insight into modulated up-conversion luminescent silica nanotubes as efficient adsorbents for colored effluents. *Dalton Transactions* **43**, 15457–15464 (2014).

125. Hu, Y. *et al.* A facile synthesis of NaYF 4 :Yb 3+ /Er 3+ nanoparticles with tunable multicolor upconversion luminescence properties for cell imaging. *RSC Advances* **4**, 43653–43660 (2014).

126. Wang, H. Q. & Nann, T. Monodisperse upconverting nanocrystals by Microwave-assisted synthesis. *ACS Nano* **3**, 3804–3808 (2009).

127. *MARS 6 Microwave Reaction System Operation Manual*. (2011).

128. Amouroux, B. *et al.* Importance of the Mixing and High-Temperature Heating Steps in the Controlled Thermal Coprecipitation Synthesis of Sub-5-nm Na(Gd-Yb)F 4 :Tm. *Inorganic Chemistry* **58**, 5082–5088 (2019).

129. Egatz-Gomez, A., Asher, M., Peterson, R., A. Roldan, M. & Ros, A. Microwave synthesis of upconverting nanoparticles with bis(2-ethylhexyl) adipate. *RSC Advances* **12**, 23026–23038 (2022).

130. Panov, N., Marin, R. & Hemmer, E. Microwave-Assisted Solvothermal Synthesis of Upconverting and Downshifting Rare-Earth-Doped LiYF4 Microparticles. *Inorg. Chem.* **57**, 14920–14929 (2018).

131. Reddy, K. L. *et al.* Amine-functionalized, porous silica-coated NaYF4:Yb/Er upconversion nanophosphors for efficient delivery of doxorubicin and curcumin. *Materials Science and Engineering: C* **96**, 86–95 (2019).

132. Homann, C. *et al.* Gum Arabic-stabilized upconverting nanoparticles for printing applications. *Optical Materials: X* **21**, 100290 (2024).

133. Nair, G. B., Tamboli, S., Kroon, R. E. & Swart, H. C. Microwave-assisted hydrothermal synthesis of LaOF:Yb3+, Ho3+ nanorods with high thermoresponsive upconversion luminescence for thermometry. *Materials Today Chemistry* **29**, 101463 (2023).

134. Wang, H. & Nann, T. Monodisperse upconversion GdF3:Yb, Er rhombi by microwave-assisted synthesis. *Nanoscale Res Lett* **6**, 267 (2011).

135. Thodhal Yoganandham, S. *et al.* Mineral and Trace Metal Concentrations in Seaweeds by Microwave-Assisted Digestion Method Followed by Quadrupole Inductively Coupled Plasma Mass Spectrometry. *Biol Trace Elem Res* **187**, 579–585 (2019).

136. Karasakal, A. Determination of Major, Minor, and Toxic Elements in Tropical Fruits by ICP-OES After Different Microwave Acid Digestion Methods. *Food Anal. Methods* **14**, 344–360 (2021).

137. Skripka, A. *et al.* Decoupling Theranostics with Rare Earth Doped Nanoparticles. *Advanced Functional Materials* **29**, 1807105 (2019).

138. Andresen, E. *et al.* Assessing the reproducibility and up-scaling of the synthesis of Er,Yb-doped NaYF4-based upconverting nanoparticles and control of size, morphology, and optical properties. *Sci Rep* **13**, 2288 (2023).

139. You, W. *et al.* Large-scale synthesis of uniform lanthanide-doped NaREF4 upconversion/downshifting nanoprobes for bioapplications. *Nanoscale* **10**, 11477–11484 (2018).

140. Chan, E. M., Gargas, D. J., Schuck, P. J. & Milliron, D. J. Concentrating and Recycling Energy in Lanthanide Codopants for Efficient and Spectrally Pure Emission: The Case of NaYF4:Er3+/Tm3+ Upconverting Nanocrystals. *J. Phys. Chem. B* **116**, 10561–10570 (2012).

141. Materia, M. E. *et al.* Multifunctional Magnetic and Upconverting Nanobeads as Dual Modal Imaging Tools. *Bioconjugate Chem.* **28**, 2707–2714 (2017).

142. Berkley Lab: Molecular Foundry. Solution Synthesis Robots. https://foundry.lbl.gov/instrumentation/solution-synthesis-robots/ (2023).

143. Xia, X., Sivonxay, E., Helms, B. A., Blau, S. M. & Chan, E. M. Accelerating the Design of Multishell Upconverting Nanoparticles through Bayesian Optimization. *Nano Lett.* **23**, 11129–11136 (2023).

144. Bateni, F. *et al.* Smart Dope: A Self-Driving Fluidic Lab for Accelerated Development of Doped Perovskite Quantum Dots. *Advanced Energy Materials* **14**, 2302303 (2024).

Funding: This research was supported by a Royal Society Research Grant (RGS\R1\221139), and a Royal Society of Chemistry Research Enablement Grant (E21-5833576777). L.M. was supported by BBSRC Discovery Fellowship (BB/T009268/1).

Acknowledgements

The picture of an autoclave used in Figure 4a was kindly provided by our colleauge Dr Juliane Simmchen (Department of Pure and Applied chemistry, University of Strathclyde, Glasgow, UK).

Author contributions:

R. McGonigle: development of PEI-UCNP methods; creation of Figure 5 and Figure 8; edited and approve the manuscript.

J. Glasgow: development of OA-UCNP methods; creation of Figure 6; edited and approved the manuscript.

C. Houston: development of PEI-UCNP methods; edited and approved the manuscript.

I. Cameron: development of PEI-UCNPs methods; edited and approved the manuscript.

C. Homan: contributed discussion of PVP-UCNPs (particularly discussion around YF_3 nanoparticles) and UCNP synthesis methods in general. Contributed to the drafting and editing of the manuscript, approved the manuscript.

D. Black assisted with characterisation of PEI-UCNPs; edited and approved the manuscript.

R. Pal assisted with characterisation of PEI-UCNPs; edited and approved the manuscript.

L.E. MacKenzie: source funding, conceived and drafted the manuscript; created all other figures, edited and proofed the manuscript.

Competing interests.

The authors declare no competing interests.